This is an unclassified edited version of NRL Rpt. 8189 by J. Baras

CONTENTS

SHIP RCS SCINTILLATION SIMULATION
[Unclassified Title]

1. INTRODUCTION

(U) Reflectivity characteristics and fluctuations of targets have been recognized as important factors in the design and performance evaluation of radar systems since the early days of radar. Reflectivity fluctuations may be due to a variety of reasons: (a) environmental conditions, (b) geometric configuration, (c) target complexity, and (d) relative motion between radar and target. In each case a "noise" process is generated that interferes with the operation of the radar system.

(U) Simulation models of radar systems have now become an important and indispensable part in various types of radar studies and design: (a) effective implementation of new concepts, (b) design of advanced radar systems, (c) performance evaluation of existing radar systems, and (d) analysis of electronic countermeasures (ECM) for radar systems. The work to be described here is primarily intended for use in conjunction with (d), where the necessity of simulation is more dramatic. However, it can easily be modified for application to any one of the other areas.

(U) One of the most pressing requirements in EW and ECM simulation is the realistic modeling of reflectivity fluctuations. The basic reason is that for some ECM techniques these fluctuations would actually improve the effectiveness of the technique [1], while for others severe deterioration may occur in the presence of certain types of fluctuations [2], [3]. In studying the effectiveness of a specific ECM technique, not only an evaluation under realistic environmental and radar-target descriptions must be provided, but in addition, all possible causes for deterioration of performance should be identified and analyzed i dependently of each other, as well as simultaneously. Since the nature and specific characteristics of the various "noise" fluctuations depend heavily on the generating mechanism, a crude "white noise type" fluctuations model would provide little if any information in ECM effectiveness evaluation. Therefore, a realistic model of each mechanism generating reflectivity fluctuations is needed and the appropriate parameters that characterize the phenomenon should be identified and analyzed.

(U) Fortunately, the major causes of reflectivity fluctuations in radar systems are well known and have been analyzed in depth, both theoretically and experimentally [4-7]. They are ([7], Ch. 28)

(1) Radar Cross Section (RCS) scintillation (fading) of targets,

(2) angle noise (glint) of targets,

(3) fluctuations due to multipath, and

(4) fluctuations due to reflections from irregular terrain.

(U) The complexity of the phenomena mentioned above is well known and the development of a realistic simulation model becomes feasible only by resorting to statistical

simulation methods. Furthermore, the intended use of the work described here dictates several "hard" constraints on the allowed complexity of the model that will be taken into account. Additions to the final models to improve realism and detail will also be presented where it is felt necessary. These latter are important for (a) use of the simulation models (to be described here) in other areas and (b) use in analyses of a more concentrated and restricted scope.

(U) The simulation models developed under this work, although of general use in ECM simulation for radar systems, were primarily developed for use as part of the NRL antiship cruise missile simulations package. As a result we are primarily interested in naval applications: the targets in (1) and (2) above are ships, multipath in (3) is over sea, and in (4) the terrain is sea. The importance of providing realistic models for (1)–(4) above, for the overall quality of a missile simulation package, is most easily demonstrated if we think of the overall missile simulation model as a problem in system identification [8–10]. The general problem in system identification is described in Fig. 1 below. The "real system" usually represents a very complex technological system which may be totally or partially unknown, or it may be known but impossible to model in a way leading to further analysis. The model usually assumes a structure and certain parameterization. K_u and K_y are memoryless processors. The objective is to match the input-output performance of the "real system" by choosing the structure and parameter values of the model (which is usually much simpler) so that a certain function of the error history is minimized. Some examples where such a formulation and the associated methodology and technology would be a fruitful approach for missile simulation problems are (a) "fine-tuning" of an existing simulation model to a new missile threat with only limited output data available, (b) test and validation of an existing simulation model, using data developed by available analog simulators or otherwise, and (c) sensitivity analysis for missile parameters and establishment of confidence limits for the overall model or parts of it. There is an important difficulty, however. System identification usually assumes u, u_M, y, and y_M are known. This is certainly not the case here, since part of u consists of

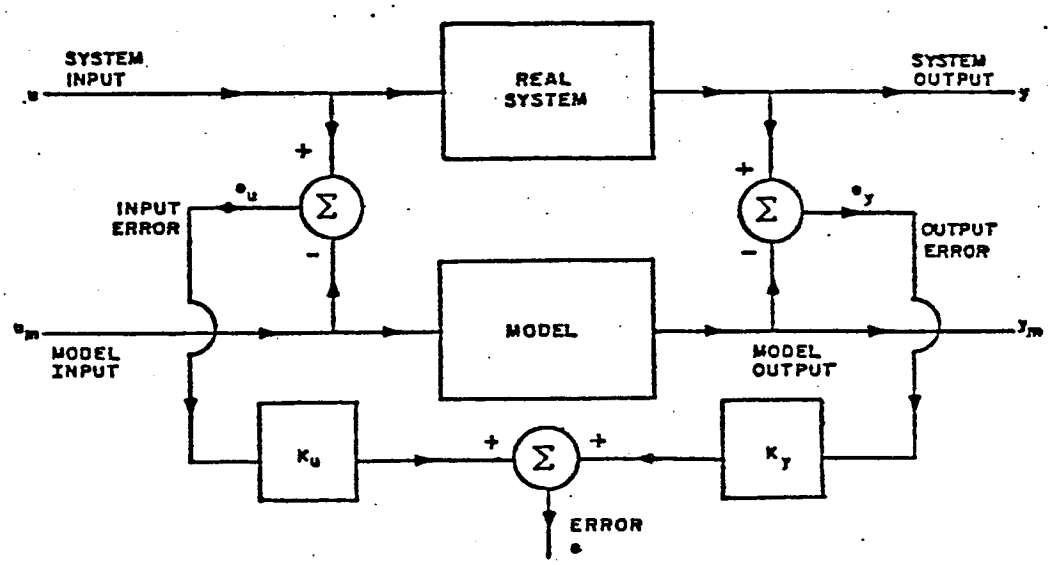

(U) Fig. 1—General system identification problem

highly complex phenomena such as target characteristics, environmental effects, and complex and varying geometries. It is also well known that input matching would generally enhance the identification (modeling) procedure. These considerations make the inclusion of models of the environment, target reflectivity scintillation, and other interference in u_M an indispensable part of any worthwhile missile simulation package.

(U) In this and companion reports [11,12] we will develop simulation models for target RCS scintillation, angle noise, multipath effects, and sea clutter. The requirements imposed on this input simulation model by the particular application intended are

(A) The underlying mathematical models should be relatively simple, so that the overall run time can be kept within reasonable limits. This is extremely important because pulse-by-pulse simulation runs are required for many ECM effectiveness evaluations.

(B) There should be a compromise between simplicity of the model and ability to represent effectively the major statistical characteristics of the "noise" processes that are simulated.

(C) The model should be *adaptive*, in the sense that the basic information needed for the operation of the model should consist of a small number of parameters for which available data bases exist or which can be easily measured experimentally. This latter is extremely important, for it allows diversified use of the model, and enables simulation results to generate suggestions for future experimental work intended to improve input matching and reliability of results obtained by the overall missile simulation package.

(D) The model should be supported by a complete list of statistical diagnostic software for validation and experimentation purposes.

(U) Most of the studies on reflectivity fluctuations are concerned with analyzing experimental data in order to identify the various "noise" processes and their most important statistical characteristics. Others develop theoretical explanations of experimental findings by utilizing scattering theory. There appears to be a lack of efforts to use this wealth of knowledge in developing simple, albeit realistic, simulation models for these "noise" processes.

(U) In this first of a series of reports, we analyze target RCS fluctuations and develop a simulation model by following the above principles.

2. RADAR CROSS SECTION OF SHIPS

(U) Complex targets (like ships) provide a variety of reflecting surfaces. A radar tracking a complex target responds to the total echo signal (skin return). Due to the complexity of shape and motion of a complex target like a ship, the total return is the vector sum of the individual returns from various parts of the target. The amplitude and phase of each individual return varies, resulting in a variation or scintillation of the overall return. These fluctuations due to the target alone are the subject of this report and partly of the companion report [11].

$$p(\sigma) = \begin{cases} \frac{1}{\bar{\sigma}} \exp\left(-\frac{\sigma}{\bar{\sigma}}\right), & \sigma \geq 0, \\ 0, & \sigma < 0, \end{cases} \tag{2.4}$$

where $\bar{\sigma}$ is the mean of σ. This is by far the most commonly used model for radar systems design, and agrees well with experimental evidence from small targets and, in particular, aircraft [4,7]. It has been found, however, unsatisfactory for many problems involving ships [15-24]. As a result, various other probability density functions have been proposed. Swerling [15,16] proposed the family of chi-square with 2m degrees of freedom and demonstrated that a large class of targets could be aequately modeled by this family:

$$p(\sigma) = \begin{cases} \frac{m}{(m-1)!\bar{\sigma}} \left(\frac{m\sigma^{m-1}}{\bar{\sigma}}\right) \exp\left(-\frac{m\sigma}{\bar{\sigma}}\right), & \sigma \geq 0, \\ 0, & \sigma < 0. \end{cases} \tag{2.5}$$

From this family, Swerling emphasized the two-degrees-of-freedom case (his cases 1 and 2, exponential or Rayleigh power, cf. Eq. (2.4)) for reasons explained above, and the four-degrees-of-freedom case (his cases 3 and 4):

$$p(\sigma) = \begin{cases} \frac{4\sigma}{\bar{\sigma}^2} \exp\left(-\frac{2\sigma}{\bar{\sigma}}\right), & \sigma \geq 0 \\ 0, & \sigma < 0. \end{cases} \tag{2.6}$$

The importance of the latter stems from the fact that it leads to detection statistics in close agreement with those derived when a steady reflection is combined with an assembly of many small reflectors. For small ships it is easy to argue that usually the total return is the sum of many independent returns, with no one dominating, resulting thus in an exponential distribution for the power return. For moderate-size and large ships, however, large reflectors exist which can dominate the return if illuminated from appropriate directions. The resulting density for the amplitude of the received field is the well-known Rice amplitude probability density function [25,26]:

$$p(\sigma) = \begin{cases} \frac{r}{\alpha^2} \exp\left(-\frac{r^2 + c^2}{2\alpha^2}\right) I_0\left(\frac{cr}{\alpha^2}\right), & r \geq 0 \\ 0, & r < 0 \end{cases} \tag{2.7}$$

where I_0 is the modified Bessel function of the first kind and order zero, c is the amplitude of the steady component, and $2\alpha^2$ is the average random power (i.e., the expected value of the square of the total amplitude of the random components). This results in a Rice-power probability density for the target RCS ([4], p. 150):

$$p(\sigma) = \begin{cases} \dfrac{1+m^2}{\bar{\sigma}} \exp\left[-m^2 - (1+m^2)\dfrac{\sigma}{\bar{\sigma}}\right] I_0\left[2m\sqrt{(1+m^2)\dfrac{\sigma}{\bar{\sigma}}}\right], & \sigma \geq 0 \\ 0, & \sigma < 0 \end{cases} \tag{2.8}$$

where m^2 is the ratio of the RCS of the steady component to the average total RCS of the random components (i.e., the ratio of the steady power to the average random power). This is the exact RCS probability density in this case, but it is seldom used because it leads to cumbersome formulas. It has been shown [18] that detection statistics based on the chi-square density with four degrees of freedom (2.6) closely approximate those based on density (2.8) with $m^2 = 1$. Therefore, Eq. (2.6) represents a good model for the RCS probability density for the case of a dominant reflector with an RCS of the same magnitude as the average sum of the RCS's of all other random components. Consequently, Eq. (2.6) can be employed in modeling small or medium-size ships. Beckner [23] arrives at this probability density from experimental observations. Finally, due to experimental evidence from large and very large ships [16,17,19,24], the lognormal probability density for ship RCS has been considered:

$$p(\sigma) = \begin{cases} \dfrac{1}{\sigma s\sqrt{2\pi}} \exp\left[-\dfrac{(\ln\sigma - \mu)^2}{2s^2}\right], & \sigma \geq 0 \\ 0, & \sigma < 0 \end{cases} \tag{2.9}$$

where s and μ are the standard deviation and mean of $\ln\sigma$. The lognormal density differs from the chi-square family of densities in that it gives higher probabilities for large values of RCS; that is, it has a higher tail. Experimentally, lognormal statistics occur whenever we have occasional very strong specular reflections, as those from flat surfaces. Large ships with large dominant scatterers produce returns at appropriate angles that often display large spikes due to the specular return from these dominant scatterers. This behavior, which results in an RCS density with higher tails, leads to the lognormal model. A possible explanation for lognormal statistics has been described in Ref. 17. It is based on the fact that the effect of surface roughness on the specular return from a flat plate is to reduce the cross section relative to that of a smooth plate by a factor of $\exp(-y)$, where y is proportional to the mean square surface depth fluctuations. If the radar return at any aspect angle is that from a surface selected from an ensemble having a normally distributed degree of roughness, lognormal statistics result. Since the return from a ship at some aspect angles is largely due to a single predominant corner, the lognormal character of ship returns could thus be explained.

(U) All types of probability densities discussed above have been observed experimentally [19–24] for the same ship under the same environmental conditions. The type of distribution changes due primarily to different aspect angles. As a result it becomes obvious that a simple model using one type of density only will be unrealistic, and therefore a model that combines various RCS probability densities is required for the statistical description of ship RCS. In order to display the difference between these densities, and in order to provide a model with meaningful transition mechanisms from one distribution

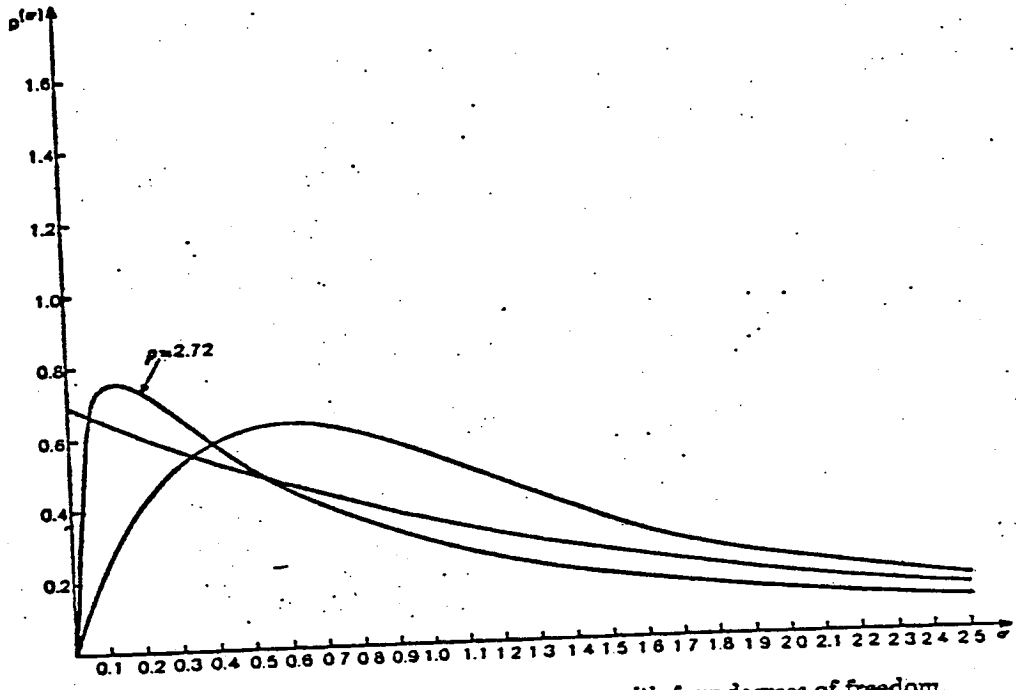

(U) Fig. 5a—Plot of exponential, chi-square with four degrees of freedom, and lognormal density with the same median = 1

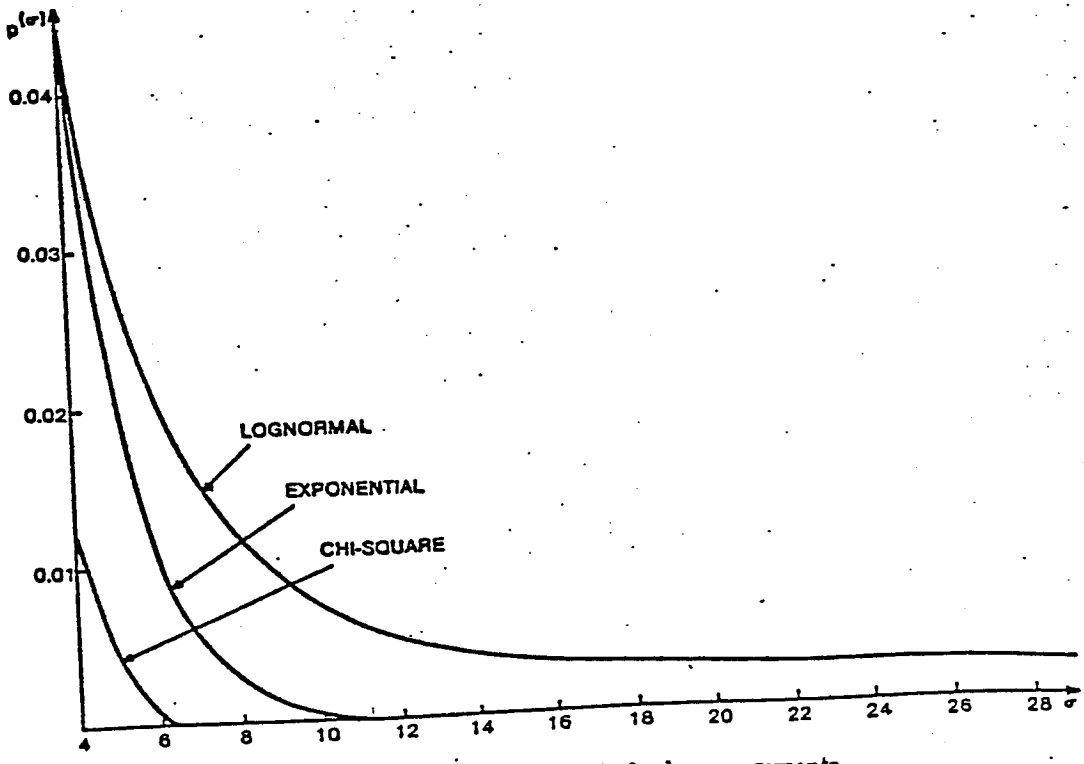

(U) Fig. 5b—Same as Fig. 5a for large arguments

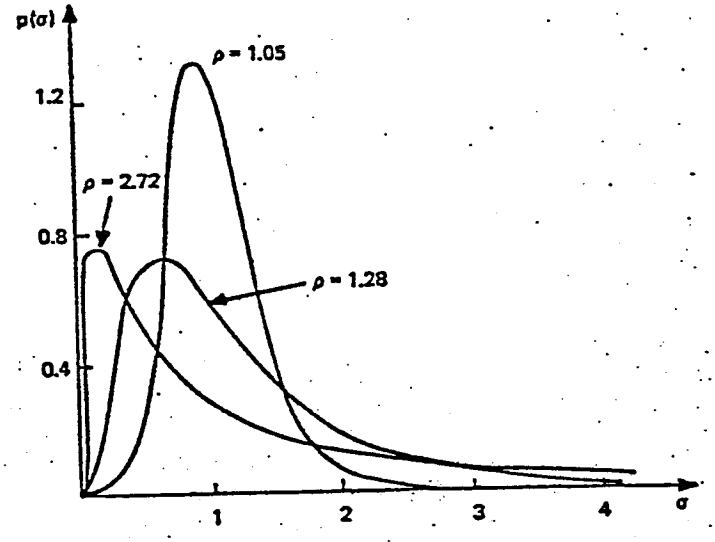

(U) Fig. 6—Lognormal probability densities with the same median $\sigma_m = 1$ and various values for ρ (from Ref. 27)

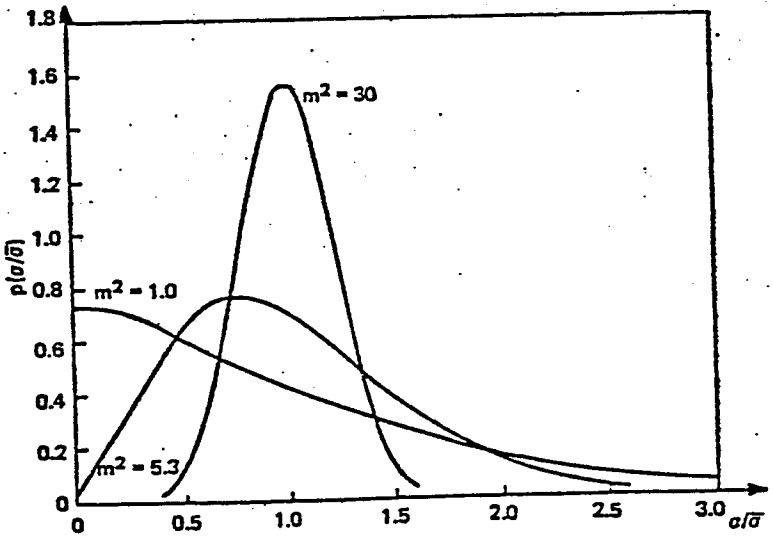

(U) Fig. 7—Rice-power probability densities for various values of m^2 (from Ref. 28)

that it is very easy to obtain a compromise in most cases studied. When one determines from experiments means, variances, and autocovariance functions, the hope is that these second-order moments will be sufficient in determining a good and realistic approximation to second-order statistics. This is the case for ship RCS fluctuations. The reason is, as we shall discuss in detail in a later section, that all probability densities we are interested in can be generated from one to four Gaussian densities by nonlinear transformations; therefore, if we can determine the appropriate second-order statistics of the underlying Gaussian processes, we will obtain a very good and realistic approximation to the second-order statistics of σ_t. In particular, we will be able to match the first-order density and the autocovariance (or autocorrelation) function, which are the usual outcomes of data processing from experimental observation of ship RCS.

(U) We now turn to a more detailed discussion of these points, which will be given in the following sections.

3. DEPENDENCE OF PARAMETERS OF RCS PROBABILITY DISTRIBUTIONS ON GEOMETRY, RADAR FREQUENCY, ETC.

(U) The first parameter we analyze is the median RCS, which as was mentioned in the previous section is widely accepted as the crucial parameter for target RCS fluctuation statistics. The median for a given target depends on the following:

(1) aspect angle between radar and target,

(2) range, and

(3) depression angle.

(U) As was explained in previous sections (we emphasize it again here), given a complex target, it is impossible to arrive at exact quantitative descriptions of these dependencies. The ideal situation from the simulation point of view is to make appropriate experiments to generate from the target enough data on which our statistical simulation model could be confidently based. Moreover, extrapolations and interpolations to other targets and geometries (the real challenge for simulation models) should be always based on adequate data. As our fundamental reference for the analysis and modeling of the dependencies above, we used the data base generated by Daley, et al. at NRL and their results as reported in Ref. 19. Additional supporting experimental evidence can be found in the reports by Beckner, et al. [20-23].

(U) First we discuss variation of the median target RCS with respect to aspect angle. Our convention for aspect angle measurement is illustrated in Fig. 8. Daley, et al. [19] collected many samples from different targets, and from different aspect angles for the same target. As part of their data processing they computed the median from samples for certain values of aspect angle and displayed the results in polar diagrams. These diagrams provide a complete description of the variation of the median RCS as a function of aspect angle. As a single number representing the target, the median of these medians was suggested. Figures 9-11 are representative polar diagrams from this work [19].

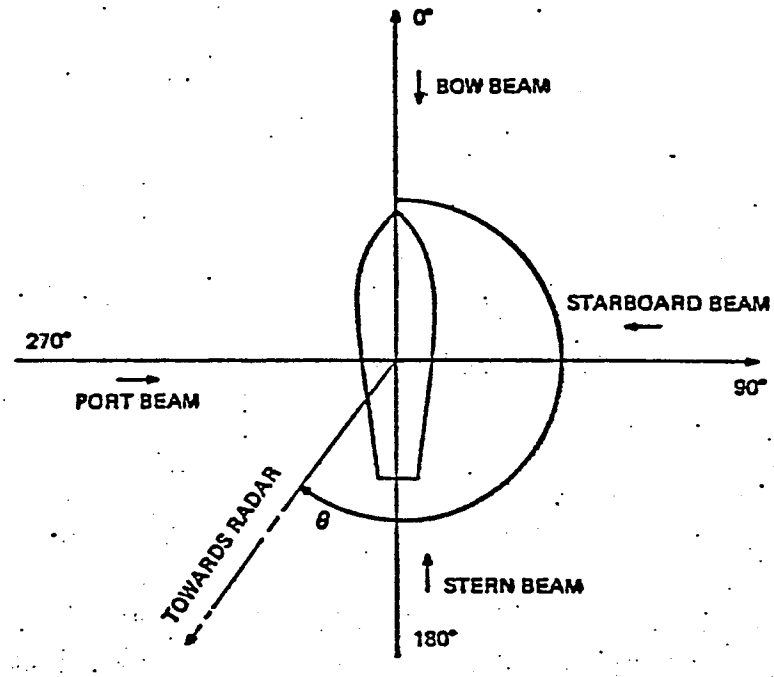

(U) Fig. 8—Convention for aspect angle

(U) If such information (i.e., such a polar diagram) is available for a particular ship, it can be employed by our simulation model whenever the simulated scenario includes this particular ship or a ship with the same characteristics. However, quite often much less information is available for a particular ship. So we need a substitute for the polar diagram which should involve a small number of parameters. To that end we summarize below the most important conclusions that can be derived from the data in Ref. 19. First, the suggested parameter, median of medians, is accepted as a representative of ship size. Next, the polar diagrams are roughly of the form shown in Fig. 12, that is, an ellipse with two peaks superimposed at starboard and port, as in Fig. 12a. In certain cases an obvious depression of the polar curve at bow aspect is observed, as in Fig. 12b.

(U) For small ships, having a median of medians roughly between 12 and 23 dB over m^2, the ellipse is kind of flat (i.e., the two axes differ considerably), the relative size of peaks is small (at the level of 4 dB), and the variation between max and min of the median RCS is roughly at the level of 10 dB (i.e., rather sizable compared to the median of medians). Furthermore, the depression around the bow aspect is more profound. For medium-size ships, median of medians roughly 25–35 dB over m^2, the ellipse is of the same type, with large relative size of peaks (at the level of 10 dB) and variation between max and min at the level of 20 dB (again considerable compared to the median of medians). In this case the change of polarization to VV or VH tends to make the ellipse more circular (i.e., equalize the two axes) and to localize the peaks very much. The depression around the bow aspect is less profound than in small ships. For large ships, having a median of medians roughly larger than 40 dB, the ellipse becomes very much like a circle (i.e., two axes almost equal), relative size of peaks is at the level of 10 dB, and variation of max to min is now at the level of 14 dB. Again, change of polarization to HV, VH, or VV reduces the relative size of peaks and also reduces the bow return to produce an asymmetry

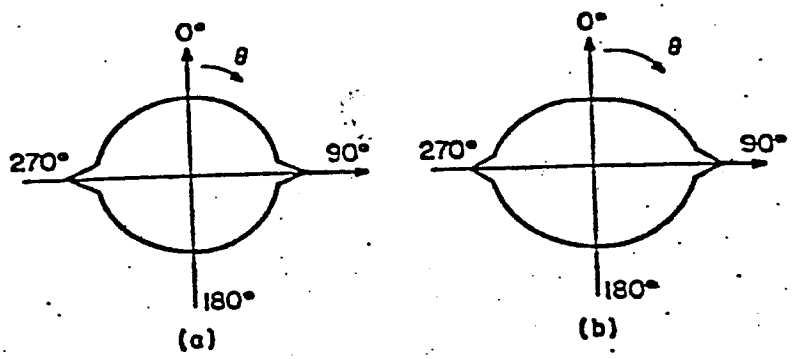

(a) and (b)

(U) Fig. 12—Approximate form of polar diagram of median RCS (in dB over m^2) vs aspect angle θ

in the polar diagram. The depression around the bow aspect is negligible. On the basis of the above, we propose two simplified polar diagrams for the variation of median RCS as function of aspect angle. The first consists of two superimposed ellipses, as shown in Fig. 13a. The parameters needed for this diagram are

(i) the median RCS at starboard and stern, σ_{mp} and σ_{ms} respectively, in dB over m^2 (if given in m^2, then $10 \log_{10} \sigma_{mp}$ and $10 \log_{10} \sigma_{ms}$ should be used),

(ii) the relative size of the peaks ΔR in dB, and

(iii) the angle ϵ where the two ellipses intersect. (3.1)

Let a_i and b_i be the two axes, $\rho_i = b_i/a_i$ the eccentricity of the inner ellipse, and a_e, b_e, and ρ_e the corresponding parameters of the other ellipse. Then

$$a_i = \sigma_{mp} - \Delta R$$

$$\rho_i = \frac{\sigma_{ms}}{a_i}$$

$$a_e = \sigma_{mp} \,. \tag{3.2}$$

The equations of the two ellipses are

$$\sin^2\theta + \frac{\cos^2\theta}{\rho_i^2} = \frac{a_i^2}{r^2(\theta)}$$

$$\sin^2\theta + \frac{\cos^2\theta}{\rho_e^2} = \frac{a_e^2}{r^2(\theta)} \,. \tag{3.3}$$

For $\theta = \epsilon$ the two amplitudes are the same, or

$$a_i^2\left[\frac{1}{\rho_i^2}+\left(1-\frac{1}{\rho_i^2}\right)\sin^2\epsilon\right]^{-1}=a_e^2\left[\frac{1}{\rho_e^2}+\left(1-\frac{1}{\rho_e^2}\right)\sin^2\epsilon\right]^{-1}$$

and

$$\frac{1}{\rho_e^2}=\left(\frac{a_e^2}{a_i^2}-1\right)\tan^2\epsilon+\frac{a_e^2}{a_i^2\rho_i^2}. \tag{3.4}$$

(U) From Eqs. (3.2) and (3.4) we calculate the parameters for the two ellipses. Then, given θ, using Eq. (3.3), we determine the median (in dB over m^2) by

$$\sigma_m(\theta)=\begin{cases} a_i\left[\frac{1}{\rho_i^2}+\left(1-\frac{1}{\rho_i^2}\right)\sin^2\theta\right]^{-1/2}, & 360^\circ-\epsilon\leq\theta<\epsilon \quad \text{and} \\ & 180^\circ-\epsilon\leq\theta<180^\circ+\epsilon, \\ a_e\left[\frac{1}{\rho_e^2}+\left(1-\frac{1}{\rho_e^2}\right)\sin^2\theta\right]^{-1/2}, & \epsilon\leq\theta<180^\circ-\epsilon \quad \text{and} \\ & 180^\circ+\epsilon\leq\theta<360^\circ-\epsilon. \end{cases} \tag{3.5}$$

(U) The second model is identical with the first, except for the replacement of the ellipse by a straight line around the bow aspect, as shown in Fig. 13b.

(U) The parameters needed for this diagram are the same as for the previous one with the addition of the median RCS at bow, σ_{mb}. Then, to determine the angle θ_B, we have from Eq. (3.3)

$$r^2(\theta_B)=a_i^2\left[1-\left(1-\frac{1}{\rho_i^2}\right)\cos^2\theta_B\right]^{-1}$$

and

$$\sigma_{mb}^2=r^2(\theta_B)\cos^2(\theta_B).$$

Therefore,

$$\sigma_{mb}^2=a_i^2\,\frac{\cos^2\theta_B}{1-\left(1-\frac{1}{\rho_i^2}\right)\cos^2\theta_B},$$

$$\frac{1}{\rho_i^2}-1+\frac{1}{\cos^2\theta_B}=\frac{a_i^2}{\sigma_{mb}^2},$$

$$\cos\theta_B=\left(\frac{a_i^2}{\sigma_{mb}^2}+1-\frac{1}{\rho_i^2}\right)^{-1/2} \tag{3.6}$$

So Eqs. (3.5) are modified to

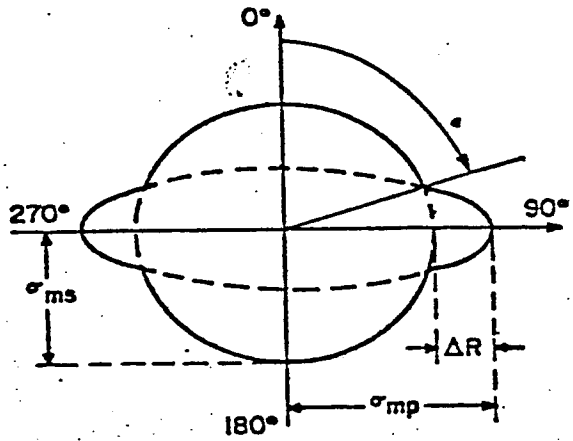

(U) Fig. 13a—Proposed simplified polar diagram for the variation of the median RCS (in dB over m^2) vs angle

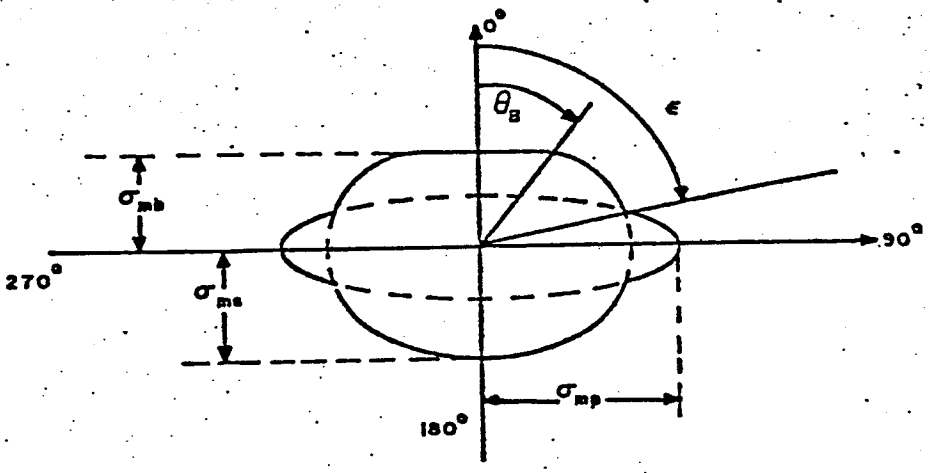

(U) Fig. 13b—Proposed simplified polar diagram with depression around bow aspect

$$\sigma_m(\theta) = \begin{cases} \sigma_{mb}/\cos\theta & , \quad -\theta_B \leq \theta < \theta_B \\ a_i\left[\dfrac{1}{\rho_i^2} + \left(1 - \dfrac{1}{\rho_i^2}\right)\sin^2\theta\right]^{-1/2} & , \quad \begin{array}{l} 360^\circ - \epsilon \leq \theta < 360^\circ - \theta_B \\ \theta_B \leq \theta < \epsilon \\ \text{and} \quad 180^\circ - \epsilon \leq \theta < 180^\circ + \epsilon \end{array} \\ a_e\left[\dfrac{1}{\rho_e^2} + \left(1 - \dfrac{1}{\rho_e^2}\right)\sin^2\theta\right]^{-1/2} & , \quad \begin{array}{l} \epsilon \leq \theta < 180^\circ - \epsilon \\ \text{and} \quad 180^\circ + \epsilon \leq \theta < 360^\circ - \epsilon. \end{array} \end{cases} \tag{3.7}$$

The selection of one of the two models depends on the size of the ship as explained above and the availability of separate data for bow and stern aspects. The graphs in Figs. 16 and 17 from Ref. 19 can also be used. This model of median RCS variation with respect to aspect angle is included in the subroutine AMERCS. The required input is described by Eq. (3.1). In cases where more accurate diagrams exist based on a detailed data base, these diagrams can be substituted in the program in lieu of the subroutine AMERCS.

(U) The dependence of median RCS on range is characterized by two phenomena. First, multipath effects produce a different value after a certain range. This results from the R^{-4} dependence of the return up to certain range, and R^{-8} dependence after certain critical range. Since most measurements are made in the R^{-4} region, we usually interpret available data as referring to this region. The multipath model in Ref. 12 will produce this change in dependence on R automatically. Second, at very close ranges when the radar beam subtends part of the ship, the values for σ_{ms}, σ_{mp}, and σ_{mb} will decrease. This change could be input to the model from available data. However, since this happens at close range only, it can be safely ignored for the purposes of the missile simulation package.

(U) When data are available, σ_{mb}, σ_{ms}, σ_{mp}, ΔR, and ϵ can be rather easily computed or estimated. If data are not available, then these target parameters should be estimated by other target parameters (such as target geometries, radar environment, etc.). In Ref. 19 various curves are given that display the dependence of median of medians on vessel length and radar frequency, etc. These curves should be used with caution to provide appropriate input to the model when data are not available.

(U) The dependence of median RCS on elevation angle becomes important at low grazing angles, and has been experimentally studied in Ref. 22, where tables with values of maximum average cross section (in the sense that the return from several range bins was measured and averaged over the number of samples obtained and the maximum of the averages was selected) as a function of depression angle for various ships can be found. The typical behavior is an increase in maximum average cross section with decreasing depression angle once it has fallen below about 4.0°. This increase at low depression angles is obviously due to the vertical surfaces of the ship being almost perpendicular to the radar

beam. In more detail, observations show that the maximum average cross section decreases as elevation increases from 0° to about 3.5°, then stabilizes, and then increases slightly again when elevation exceeds 9°–10° as returns from the deck influence the total return. Since for low elevation angles multipath effects are present, the separation of the two phenomena becomes extremely difficult. Our primary interest is for elevation angles from 0° to 10°. In Table 1, examples of this variation are given from Ref. 22.

(U) Removing fades that are obviously due to multipath, we see that a linear decrease of maximum average RCS (in dB over m^2) as a function of elevation angle between 0.5° and 3.5° fits these data rather well, as shown in Fig. 19. Below 0.5°, a flattening of the curve is observed from USS *Norton Sound* data. This is expected because at very low grazing angles the radar beam is perpendicular to the flat vertical scatterers, causing the phenomenon, and further increase of the RCS should not be observed as the elevation decreases even further. As a result of these observations, a flat, decreasing parabola with maximum at zero is proposed as an appropriate curve to fit the limited data base available. The flatness of the parabola depends on the structure of the ship; in particular, on the existence of dominant scatterers of the large flat vertical plate type. The more and larger scatterers of this type exist, the more profound the increase due to decrease in elevation angle must be, resulting in a less flat parabola. Indeed, from photographs in Ref. 22 we observe that USS *Norton Sound*, a guided-missile ship, displays large and high flat plates on its sides, while USS *Southerland* is a typical destroyer with fewer and smaller reflectors of this type. From Fig. 19 we see that the parabola for USS *Southerland* is flatter than the parabola for USS *Norton Sound*. The flatness of the parabola depends also on the wavelength of the radar, because the smaller the wavelength, the larger the apparent dimensions of the flat scatterer.

(U) On the basis of the above, we propose the following model for the variation of median RCS as a function of elevation angle. If we express the median in dB over m^2, its variation with respect to elevation angle is parabolic, as shown in Fig. 20 below. Here, σ_m is the value associated with the ship at the particular aspect angle we are considering, as discussed earlier in this section. The value of κ depends on the proportion and orientation of large flat plate-type scatterers that a particular ship has, and therefore depends on aspect angle. It is expected that, typically, κ has its maximum value at port and starboard and is monotonically decreasing as we move away from these aspect angles. Furthermore, it is believed that κ depends primarily on the height of flat perpendicular plates as seen from various aspect angles. Clearly, if appropriate data are available, the value of κ and

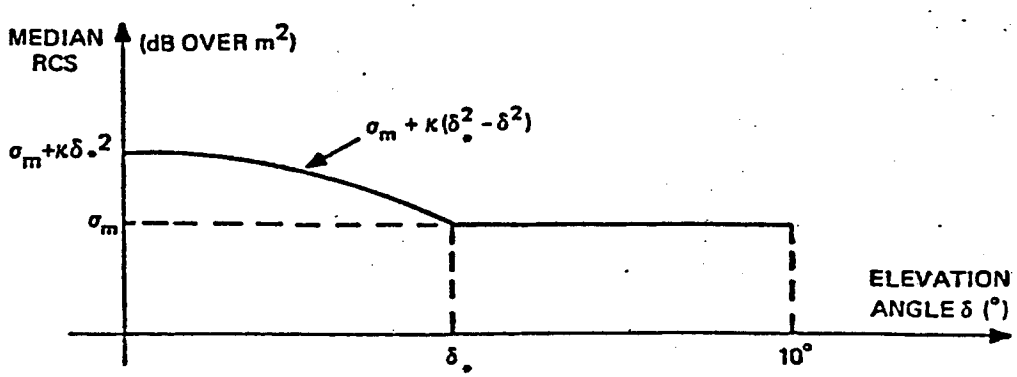

(U) Fig. 20—Proposed simplified variation of median RCS with respect to elevation angle

the angle where the median becomes constant (see Fig. 20) can be determined as functions of aspect angle. Care should be exercised at very low depression angles to avoid fadings due to multipath effects. This is obviously a crude model based on the limited data available for this phenomenon. Further data will certainly provide for improvements. The recommended value for δ_* is 3.5°.

(U) From the theoretical point of view, one can resort to approximate calculations due to scattering from a flat plate. If we consider a flat plate as shown in Fig. 21, the field pattern, based on far-field approximations, is given by [7,9-7]

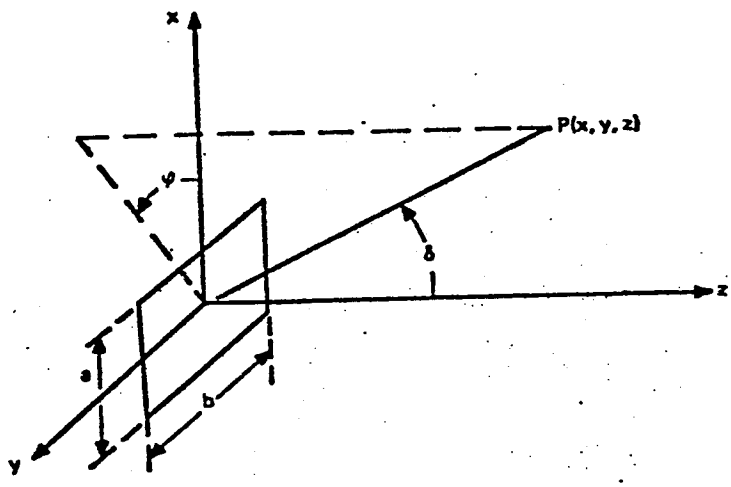

(U) Fig. 21—Flat plate scattering geometry

$$F(\theta, \phi) = \frac{\sin\left[(\pi a/\lambda)\sin\delta\cos\phi\right]}{(\pi a/\lambda)\sin\delta\cos\phi} \cdot \frac{\sin\left[(\pi b/\lambda)\sin\delta\sin\phi\right]}{(\pi b/\lambda)\sin\delta\sin\phi}. \tag{3.8}$$

Therefore, the far-field power pattern is proportional to $(\sin u/u)^2$, $u = (\pi a/\lambda)\sin\delta$, for the principal plane xz. For small elevation angles δ, the resulting power pattern has the form (using a Taylor series expansion) in dB over the maximum (for $\theta = 0$):

$$P(\delta) = -\text{const}\,\frac{a^2}{\lambda^2}\,\delta^2 .$$

This implies a variation of the median of the form (in dB over m^2)

$$\sigma_m(\delta) = \sigma_m^{\max} - C\,\frac{a^2}{\lambda^2}\delta^2 \tag{3.9}$$

where C is a constant. Therefore these approximate calculations support the behavior observed from the data. Indeed, since

$$\sigma_m(\delta_*) = \sigma_m = \sigma_m^{\max} - C\,\frac{a^2}{\lambda^2}\,\delta_*^2 ,$$

we can rewrite this approximate theoretical model in exactly the form that was suggested from the data:

$$\sigma_m(\delta) = \sigma_m + C\,\frac{a^2}{\lambda^2}\,(\delta_*^2 - \delta^2). \tag{3.10}$$

In Eq. (3.10), $C(a^2/\lambda^2)$ corresponds to the parameter κ of Fig. 20 and should by no means be interpreted as implying a $1/\lambda^2$ dependence of σ_m (the constant C may as well depend on λ). Whenever data are not available, Eq. (3.10) can be used to provide a reasonable

model. The angle δ_* should be selected typically between 3° and 4°. The parameter a should represent a characteristic height of the ship for this aspect angle (e.g., height of the hull). Finally, C should be estimated on the basis of the proportion of large flat scatterers that exist in this aspect angle. This model of median RCS variation with respect to elevation angle is included in the subroutine EMERCS.

(U) For the two parameter densities, i.e., Rice power and lognormal, we need to specify another parameter. We choose m^2 (the ratio of steady to average random power) or variance for Rice power, and ρ (mean to median ratio) or variance for lognormal. When data are available, the most reliable procedure is to determine the variance of RCS variation with respect to aspect angle and input it to the model. When data are not available, an estimate of m^2 or ρ should be computed from considering the shape of the target, aspect angle, etc. (see also section 2).

(U) To satisfy our constraint of a piecewise wide-sense stationary statistical model, care should be exercised in simulation so that these parameters are updated at appropriate intervals only.

4. SPECTRAL DENSITY OF SHIP RCS FLUCTUATIONS

(U) As was explained in section 2, the power return fluctuations are due to the change in relative phase of the individual returns. The power spectral density is therefore related to the rate of change of the relative phase. To see this, consider the simple case of an oriented beam with two reflectors separated by distance L, which is rotating around its center (see Fig. 22a). Let us suppose that the two reflectors are identical spheres. Then the amplitude of the combined return will be

$$A(t) = C\{\exp[j\phi_1(t)] + \exp[j\phi_2(t)]\}, \tag{4.1}$$

where C is the amplitude return when one sphere is located at the center of the beam, and $\phi_1(t)$ and $\phi_2(t)$ are the relative phases of the amplitude returns from the two reflectors with respect to the return from a sphere located at the center of the beam. Therefore the power return has the form

$$P(t) = C_1[1 + \cos\phi(t)]. \tag{4.2}$$

Here $\phi(t)$ is the relative phase between the two reflectors and is given by

$$\phi(t) = -\frac{4\pi L}{\lambda}\cos\theta(t), \tag{4.3}$$

where λ is the wavelength of the transmitted radiation. It is obvious that the harmonic content of the power return is related to the rate of change of the relative phase $\phi(t)$. If the beam is not moving, the return will not fluctuate. On the other hand, if the motion is such that $\phi(t)$ is of the form $\omega^* t$, then the spectral density for Eq. (4.2) will be

$$\frac{\pi}{2} C_1^2[\delta(\omega - \omega^*) + \delta(\omega + \omega^*)],$$

where $\delta(\cdot)$ is a delta function. Although not precisely correct, $\omega^* = d\phi(t)/dt$ can be considered in this case the "bandwidth" of the spectral density of Eq. (4.2). Next consider the same beam, but with a number of such pairs of spheres symmetrically located about its center at distances L_i, as shown in Fig. 22b. Suppose that the motion is such that $\cos\theta(t) = \omega^* t$. Then for each pair of spheres the previous discussion applies and the power due to this pair will be

$$P_i(t) = C_i[1 + \cos\phi_i(t)] \tag{4.4}$$

where

$$\phi_i(t) = -\frac{4\pi L_i}{\lambda}\omega^* t\,. \tag{4.5}$$

In addition, if we have chosen L_i such that

$$\frac{4\pi L_i}{\lambda} = i\,, \quad i = 1, 2, \ldots, n\,, \tag{4.6}$$

then Eq. (4.5) results in

$$\phi_i(t) = -i\omega^* t\,. \tag{4.7}$$

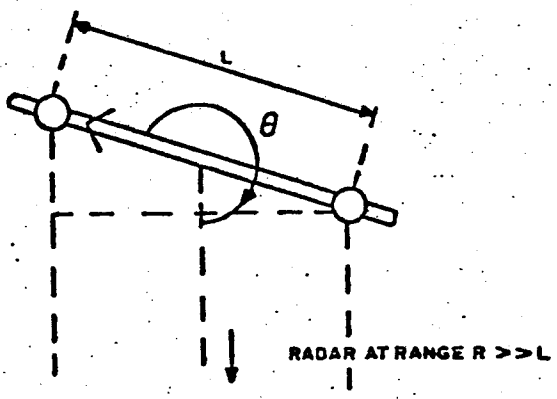

(U) Fig. 22a—Illustrating a simple example

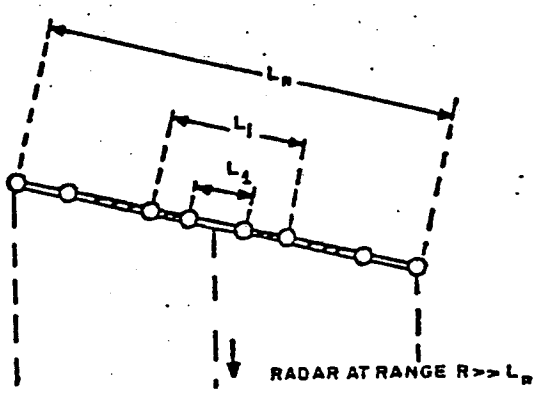

(U) Fig. 22b—Illustrating approximate derivation of bandwidth

As a result, the power spectral density of the power return from the beam will show peaks at the frequencies $i\omega^*$, $i = 1, \ldots, n$, and will drop considerably for $\omega > n\omega^*$. Again, if we assume that all spheres have the same RCS, $n\omega^* = d\phi(t)/dt$ is a reasonable approximation to the "bandwidth" of the spectral density of the total power return. As a result of such typical arguments, a usual approximation is to conclude that for distributed scatterers on such a beam with symmetry around its center, the half-power bandwidth is closely approximated by the average value of

$$\frac{1}{2\pi}\dot{\phi}(t) = \frac{2\dot{l}}{\lambda}. \tag{4.8}$$

where l is the length of the projection of the rotating beam on the direction of the radar beam. Depending on the distribution of targets on the beam, l may be the projection of that certain portion of the beam which contains the most significant scatterers.

(U) For a complex target like a ship, the situation is more complicated due to the different rates of change of relative phase between the various reflectors of the distributed target. Experiments indicate ([4], p. 173–183), ([5], p. 82 and p. 323) that the power spectral density of the ship RCS fluctuations due to deterministic and random azimuth (aspect), pitch, and roll motion can be very well approximated by a power spectral density of the form

$$S(f) = \frac{Af_B}{f_B^2 + f^2}, \tag{4.9}$$

where f_B is the half-power bandwidth in Hz and f is the frequency in Hz. Further experimental evidence for this form of power spectral density is provided in Refs. 20–23.

(U) The following arguments provide theoretical support for the proposed spectral density type. Typically, "amplitude noise" (i.e., the RCS fluctuations) from complex targets falls in two categories: low-frequency and high-frequency noise ([7], 28-3). The low-frequency portion of the noise is due to small changes in the relative phases of the returns from various reflectors as the target moves in a deterministic and/or random fashion in yaw, pitch, and roll. Typically, and this is particularly true for ships, this motion creates only small aspect changes and therefore the amplitudes of the returns vary little over a period of seconds, leaving the change in relative phase as the major reason for the fluctuating return ([7], 28-3). On the other hand, the high-frequency portion of the noise contains random noise and periodic modulation. The random noise is due to vibrating parts of the target, while periodic components are introduced by rotating parts. Both motions appear usually in aircrafts, while ships do not usually display vibrating or rotating parts. As a result, high-frequency "amplitude noise" is primarily associated with aircraft, and the corresponding components have been experimentally observed in power spectral densities of aircraft RCS fluctuations ([7], 28-7). Since our interest lies in ships, we see that only low-frequency "amplitude noise" appears. The shape of the spectral density reflects the distribution of scatterers from the target. Furthermore, the deterministic motion of a ship in azimuth and its random motion in azimuth, pitch, and roll are slow phenomena. As a result, most of the harmonic components should be concentrated at low frequencies. Indeed, experimental evidence [20–23] establishes that the typical half-power bandwidth is at the level of 10–15 Hz or less. If the

spectral density has a peak at a frequency $f^* > 0$, this will indicate a periodic component due to the change in relative phase of the amplitude returns from two dominant symmetrically located scatterers on the ship. This is not the case for ships for the following reasons: (a) the major portion of the fluctuations is due to the random motion of dominant scatterers (such as large plates), and it is very improbable that there can be an almost periodic motion between two such scatterers, and (b) the ship's random motion in pitch and roll due to sea waves provides a large portion (as compared to yaw motion) of the change in relative phase between reflectors, and this motion is not periodic and is not compatible with the ship's major symmetries. Furthermore, due to the usual structure of ships, dominant scatterers undergo slower and smaller displacements than smaller scatterers. Therefore, a bell-shaped power spectral density with maximum at zero frequency is expected for ship RCS fluctuations.

(U) The autocovariance function corresponding to the spectral density (4.9) is

$$R(t) = R \exp(-t/t_c), \tag{4.10}$$

where

$$t_c = \frac{1}{2\pi f_B} \tag{4.11}$$

is the correlation time and R is the variance of the RCS fluctuations. Since R is determined by the distribution of RCS (see section 2), we only need specify t_c (or f_B). In general, the bandwidth f_B will depend on

(i) aspect angle,

(ii) distribution of dominant scatterers on ship,

(iii) radar frequency, and

(iv) rate of change of aspect, elevation, and roll angle (an average rate), deterministic and random.

The reason for (iii) is obvious: a given change in relative range between two scatterers on the target will subtend more wavelengths for shorter wavelengths, causing a higher phase rate and thus higher frequency components. From experimental evidence ([7], 28-5), the dependence of bandwidth f_B on RF is linear. Beckner et al. [20] studied experimentally the dependence of spectral bandwidth on aspect angle. Figure 23 shows a histogram for this dependence. From the histogram a sinusoidal dependence on aspect angle can be detected.

(U) In Ref. 4, p. 174, the following formula is suggested for the bandwidth:

$$f_B = K\left(\frac{L_0}{\lambda}\right)\left(\frac{\Delta\theta}{\Delta t}\right), \tag{4.12}$$

where K is a constant of proportionality with typical value 2, L_0 is the length of the target as projected along the radar-target line, λ is the wavelength of the transmitted radiation, and $\Delta\theta/\Delta t$ is the average rate of change of aspect angle due to systematic and

random motions. A similar formula was proposed in Ref. 22, p. 108, and calculations on the basis of the formula were compared with calculations from data. In general, good agreement was found as shown in Figs. 24, 25, and 26. We note that formula (4.12) incorporates the expected dependence on geometry, environment (sea condition), and radar frequency discussed earlier in this section.

(U) In Ref. 22, formula (4.12) was derived by following exactly the kind of approximation discussed in the beginning of this section, which leads to Eq. (4.8). We give now a somewhat more detailed calculation. The geometry of the radar engagement is shown in Fig. 27. The two axes x_s and y_s are on the surface of the sea and represent the average horizontal plane; x_s is oriented according to the forward motion of the ship. δ_s indicates the pitch of the ship due to the sea waves and is a random motion; ϕ_s similarly is random and indicates the roll of the ship due to sea waves. δ denotes the elevation between radar and ship; it has a deterministic component due to the relative systematic ship-missile motion and a random component due to the random motion of the ship due to sea waves and to random fluctuations in the missile's altitude. In accordance with the approximation discussed above, the ship is modelled by two perpendicular beams of lengths L and W, respectively. The length L should be chosen according to the longitudinal distribution of scatterers on the ship. For small and medium-size ships, L should be chosen as the distance between forward and rear gun turrets (or missile-firing turrets). If no such structure exists (e.g., submarines, auxiliary vessels, etc.), L should be chosen as the length of the ship. For large and very large ships, L should equal the length of the ship also. The length W should be chosen according to the distribution of scatterers across the ship as viewed from bow or stern beam. Usually, W should be equal to the width of the ship. According to Eq. (4.8), we need to compute the projection of L or W onto the radar-ship direction. Let these projections be denoted by l and w. Then

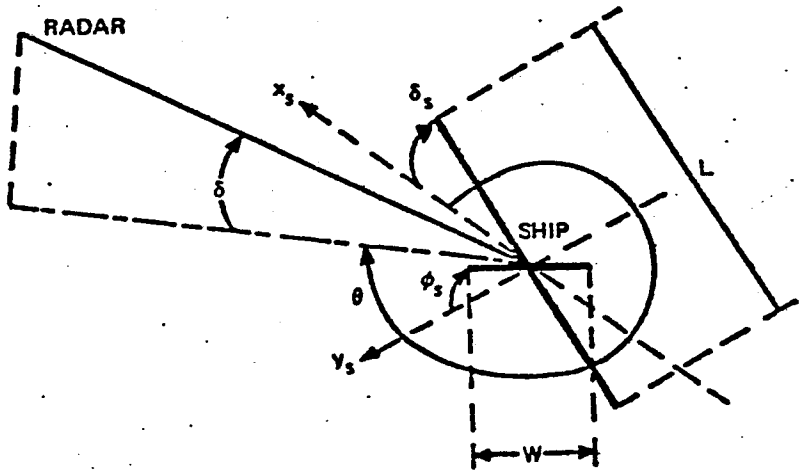

(U) Fig. 27—Radar geometry for approximate calculation of RCS fluctuations bandwidth

$$l = L(\cos\theta \cos\delta \cos\delta_s + \sin\delta \sin\delta_s) \tag{4.13}$$

and

$$\frac{2\dot{l}}{\lambda} = \frac{2L}{\lambda}\left(-\sin\theta \cos\delta \cos\delta_s \frac{d\theta}{dt} - \cos\theta \sin\delta \cos\delta_s \frac{d\delta}{dt}\right.$$

$$-\cos\theta \cos\delta \sin\delta_s \frac{d\delta_s}{dt} + \cos\delta \sin\delta_s \frac{d\delta}{dt}$$

$$\left.+\sin\delta \cos\delta_s \frac{d\delta_s}{dt}\right). \tag{4.14}$$

Since under the same environmental conditions the average rate, over a relatively short time interval, should be the same for symmetrical positions of the ship with respect to the radar-ship direction, and because we actually want to compute an average value for Eq. (4.14), we propose the following formula for this "average":

$$\omega_{BL} = \left(\frac{2\dot{l}}{\lambda}\right)_{ave} = \frac{2L}{\lambda}\left[|\sin\theta| \cos\delta \cos\delta_{sm} \frac{\Delta\theta}{\Delta t}\right.$$

$$+(|\cos\theta| \sin\delta \cos\delta_{sm} + \cos\delta \sin\delta_{sm}) \frac{\Delta\delta}{\Delta t}$$

$$\left.+(|\cos\theta| \cos\delta \sin\delta_{sm} + \sin\delta \cos\delta_{sm}) \frac{\Delta\delta_s}{\Delta t}\right] \tag{4.15}$$

where δ_{sm} is the rms pitch angle. The rates of change of the various angles represent averages over appropriate intervals of time. $\Delta\theta/\Delta t$ consists of two parts: a deterministic one that can be computed from the motions of the missile and the ship, and a random one. The same is true for $\Delta\delta/\Delta t$. The random components of $\Delta\theta/\Delta t$, $\Delta\delta/\Delta t$, the rate $\Delta\delta_s/\Delta t$, and δ_{sm} should be estimated from sea condition, ship size, wind speed, and wave height (or from existing data). Notice that if we assume that δ and δ_s are very small and slowly varying, Eq. (4.14) results in Eq. (4.12).

(U) From Fig. 27 we also find

$$w = W(-\sin\theta \cos\delta \cos\phi_s + \sin\delta \sin\phi_s) \tag{4.16}$$

and

$$\frac{2\dot{w}}{\lambda} = \frac{2W}{\lambda}\left(\cos\theta \cos\delta \cos\phi_s \frac{d\theta}{dt} + \sin\theta \sin\delta \cos\phi_s \frac{d\delta}{dt}\right.$$

$$+\sin\theta \cos\delta \sin\phi_s \frac{d\phi_s}{dt} + \cos\delta \sin\phi_s \frac{d\delta}{dt}$$

$$\left.+\sin\delta \cos\phi_s \frac{d\phi_s}{dt}\right). \tag{4.17}$$

Following similar arguments as those leading to Eq. (4.15), we derive the following "average" of Eq. (4.17):

$$\omega_{BW} = \left(\frac{2\dot{w}}{\lambda}\right)_{\text{ave}} = \frac{2W}{\lambda}\Bigg[\,|\cos\theta|\cos\delta\cos\phi_{sm}\,\frac{\Delta\theta}{\Delta t}$$

$$+(|\sin\theta|\sin\delta\cos\phi_{sm}+\cos\delta\sin\phi_{sm})\frac{\Delta\delta}{\Delta t}$$

$$+(|\sin\theta|\cos\delta\sin\phi_{sm}+\sin\delta\cos\phi_{sm})\,\frac{\Delta\phi_s}{\Delta t}\Bigg], \tag{4.18}$$

where ϕ_{sm} is the rms roll angle. The parameters ϕ_{sm} and $\Delta\phi_s/\Delta t$ should be estimated in a similar fashion as δ_{sm} and $\Delta\delta_s/\Delta t$. Finally, our formula for the bandwidth (in rads/s) is

$$\omega_B = \max(\omega_{BL}, \omega_{BW}). \tag{4.19}$$

Formula (4.19) remedies the disagreement of formula (4.12) with experimental data from bow and stern aspect in particular (formula (4.12) predicts zero bandwidth). This disagreement is due to the fact that for bow and stern aspects, it is the relative motion of scatterers distributed across the width of the ship, and not along the ship, that causes RCS fluctuations. This is particularly so for low grazing angles.

(U) Summarizing, the autocovariance function of ship RCS fluctuations will be modeled by Eq. (4.10). R will be assigned a value as discussed in sections 3 above and 5 following. For the correlation time we have two options:

A. If adequate pulse-to-pulse data are available, compute t_c for various aspect and elevation angles and input to the simulation model.

B. If such data are not available, use the following procedure:

(i) Estimate average random rate of change of aspect angle, elevation angle, ship's pitch, ship's roll, and rms pitch and roll angles of the ship based on ship size, wave height, sea state, and wind speed.

(ii) Compute ω_B from Eqs. (4.15), (4.18), and (4.19). Set

$$t_c = \frac{1}{\omega_B}. \tag{4.20}$$

Since option B above provides only an approximate model, some preliminary calculations are suggested to ensure that the resulting values for the correlation time are reasonable. A good check is to ascertain that the bandwidth remains below 25 Hz for all values of the parameters. Obviously, experience in the utilization of the model and comparison with computations based on the data base in Ref. 19 will provide useful information for the values of these parameters. Work on this is in progress and the results will be reported elsewhere.

and a diffuse-type RCS (see Eq. (5.11) following and related discussion). Two aspect angle ranges where the distribution is clearly of a particular type (one of the four used), but different in each range, are separated from each other by an angle sector where the distribution type is undetermined.

(U) Based on the above, we propose the following model for simulating the variation of distribution type.

(1) Decide what distributions to use according to the following:

(a) if extensive pulse-by-pulse data are available for a similar class ship, estimate probability densities from data at various aspect angles to find the types of densities needed.

(b) if such data are not available, then

(i) for small ships (according to our classification in section 3), use exponential (Rayleigh power) density for all aspect angles. If from known structure of the ship (or photographs) it is apparent that dominant scatterers exist at starboard and port, use also chi-square with four degrees of freedom or Rice power. Chi-square should be preferred if an appropriate value for the parameter m^2 of the Rice density cannot be determined.

(ii) For medium-size ships, use lognormal or chi-square with four degrees of freedom or Rice power around starboard and port. Lognormal should be used if flat dominant scatterers exist and are the usual situation. Use exponential for quarter aspects in most cases. Use of chi-square with four degrees of freedom or Rice power for quarter aspects is rare and is suggested only if dominant directive scatterers exist in these directions. For bow or stern, use any one of exponential, chi-square with four degrees of freedom, or Rice power, according to the aforementioned rules.

(iii) For large ships, use lognormal around major aspect angles (starboard, port, bow, stern). If major flat scatterers do not exist at bow or stern, use chi-square with four degrees of freedom or Rice power. Use exponential, chi-square with four degrees of freedom, or Rice power at quarter aspects according to the rules explained in (ii) above.

(2) Draw a polar diagram indicating the angle sectors where the distribution is to be of a particular type, using the results of (1) above, according to the following:

(a) if extensive pulse-by-pulse data are available for a similar class ship, compute the extent of the various aspect angle sectors from these data.

(b) if such data are not available, then we let p_{ma} and p_{qa} denote the probability density types, selected in (1) above for major aspect and quarter aspect angles, for the ship under consideration. By careful consideration of the distribution, orientation, and type (i.e., flat or not) of dominant scatterers on the ship, and using the results of Table 6 in Ref. 19 for guidance, estimate the percentage of distributions that are of type p_{ma} or p_{qa}. Let

(U) Finally, since the primary factor influencing the value of correlation time is aspect angle, the value of correlation time is changed at intervals determined by change of aspect angle by a specified predetermined angle. Although the optimal updating should be determined by "tuning" the model to data, a value of 2° for the necessary change in aspect angle was found to be more than adequate. This updating is in agreement with our basic piecewise wide-sense stationary approximation.

5. VARIATION OF PROBABILITY DENSITY OF SHIP RCS FLUCTUATIONS

(U) In section 2 we explained why a statistical model incorporating various probability densities is necessary for realistic simulation of ship RCS fluctuations. In this section we provide a detailed description of the proposed model for the variation of the probability density type due to ship size, structure, and aspect angle.

(U) Our proposed model is based on extensive data analyses results from Daley et al. [19] and Beckner et al. [20-23]. The following are the major conclusions from a careful consideration of their results:

(i) Lognormal statistics appear at major aspect angles, i.e., starboard, port, stern, bow. The reason (see also sections 2 and 3) is that lognormal statistics are due to dominant flat scatterers which appear mainly at these aspects.

(ii) The aspect angle range around starboard or port where lognormal statistics occur is larger than the corresponding range around bow or stern. The reason again is rather obvious: more and larger dominant flat scatterers are distributed alongside the ship than across it.

(iii) For small ships, according to our classification given in section 3, most of the observed distributions are Rayleigh power (exponential). A small percentage of distributions are well approximated by chi-square with four degrees of freedom or Rice power. For medium-size ships, all four density types proposed in section 2 have been observed. However, lognormal statistics appear only at starboard and port aspects and not at bow and stern aspects. For large and very large ships, all four density types have been observed. Lognormal statistics have been observed at all four major aspect angles (e.g., aircraft carrier) or at the two major aspect angles (e.g., battleship). In Ref. 19, p. 45, Table 6 provides the percentages of distributions observed that were shown to belong to one of these types by statistical tests.

(iv) At quarter aspects, statistics are exponential (Rayleigh power) for small ships, chi-square with four degrees of freedom or Rice power or exponential (Rayleigh power) for medium-size and large ships.

(v) There are aspect angle ranges, symmetrically distributed, where the distribution type cannot be clearly determined according to statistical tests. For these aspect angles, the distribution is a mixture of two distributions. The reason for this is that at these aspect angles, the power return is partly due to return from dominant scatterers (such as at major aspect angles) and partly due to diffuse return (such as at quarter aspect angles). The contribution from each reflection type depends obviously on aspect angle. This results in an RCS which is a convex combination of a dominant scatterer-type RCS

and a diffuse-type RCS (see Eq. (5.11) following and related discussion). Two aspect angle ranges where the distribution is clearly of a particular type (one of the four used), but different in each range, are separated from each other by an angle sector where the distribution type is undetermined.

(U) Based on the above, we propose the following model for simulating the variation of distribution type.

(1) Decide what distributions to use according to the following:

(a) if extensive pulse-by-pulse data are available for a similar class ship, estimate probability densities from data at various aspect angles to find the types of densities needed.

(b) if such data are not available, then

(i) for small ships (according to our classification in section 3), use exponential (Rayleigh power) density for all aspect angles. If from known structure of the ship (or photographs) it is apparent that dominant scatterers exist at starboard and port, use also chi-square with four degrees of freedom or Rice power. Chi-square should be preferred if an appropriate value for the parameter m^2 of the Rice density cannot be determined.

(ii) For medium-size ships, use lognormal or chi-square with four degrees of freedom or Rice power around starboard and port. Lognormal should be used if flat dominant scatterers exist and are the usual situation. Use exponential for quarter aspects in most cases. Use of chi-square with four degrees of freedom or Rice power for quarter aspects is rare and is suggested only if dominant directive scatterers exist in these directions. For bow or stern, use any one of exponential, chi-square with four degrees of freedom, or Rice power, according to the aforementioned rules.

(iii) For large ships, use lognormal around major aspect angles (starboard, port, bow, stern). If major flat scatterers do not exist at bow or stern, use chi-square with four degrees of freedom or Rice power. Use exponential, chi-square with four degrees of freedom, or Rice power at quarter aspects according to the rules explained in (ii) above.

(2) Draw a polar diagram indicating the angle sectors where the distribution is to be of a particular type, using the results of (1) above, according to the following:

(a) if extensive pulse-by-pulse data are available for a similar class ship, compute the extent of the various aspect angle sectors from these data.

(b) if such data are not available, then we let p_{ma} and p_{qa} denote the probability density types, selected in (1) above for major aspect and quarter aspect angles, for the ship under consideration. By careful consideration of the distribution, orientation, and type (i.e., flat or not) of dominant scatterers on the ship, and using the results of Table 6 in Ref. 19 for guidance, estimate the percentage of distributions that are of type p_{ma} or p_{qa}. Let

r_{ma} = fraction of distributions of type p_{ma},

r_{qa} = fraction of distributions of type p_{qa}. (5.1)

Let ϵ_s and ϵ_p be the aspect angle sectors (in degrees) around stern-bow and starboard-port where p_{ma} occurs, as shown in Fig. 28. Let L_d and W_d be characteristic lengths of the ship, representing the length of flat dominant scatterers alongside and across the ship, respectively. Typically, L_d will be equal to the length, and W_d, to the width of the ship. Then a rough scattering approximation for ranges much larger than the physical dimensions of the ship indicates that

$$\frac{\tan \epsilon_p}{\tan \epsilon_s} = \frac{L_d}{W_d}. \tag{5.2}$$

Finally, let

r_T = fraction of distributions of undetermined type

$$= 1 - r_{ma} - r_{qa} \tag{5.3}$$

and ϵ_T be the aspect angle sector where the distribution is not of a specified type, as shown in Fig. 28. We wish to compute the angles ϵ_p, ϵ_s, and ϵ_T from the parameters r_{ma}, r_{qa}, L_d, and W_d. In view of the obvious symmetry of Fig. 28, we have

$$\epsilon_p + \epsilon_s = 90 r_{ma} \tag{5.4}$$

$$90 - \epsilon_p - \epsilon_s - 2\epsilon_T = 90 r_{qa}. \tag{5.5}$$

Now Eqs. (5.2), (5.4), and (5.5) result in

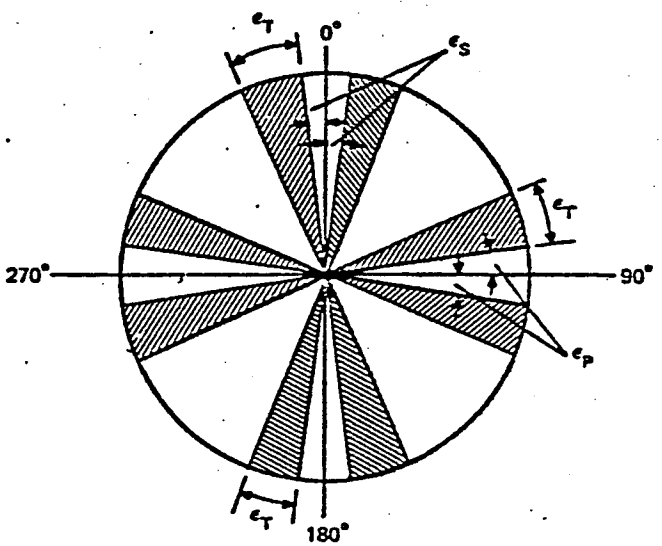

(U) Fig. 28—Aspect angle sectors with distribution type

$$\epsilon_p = \arctan\left(\frac{-1 - \frac{W_d}{L_d} + \sqrt{(1 + W_d/L_d)^2 + 4\tan^2\varphi\, W_d/L_d}}{2\tan\phi\, W_d/L_d}\right),$$

where

$$\phi = 90 r_{ma}\,, \tag{5.6}$$

$$\epsilon_s = 90 r_{ma} - \epsilon_p\,, \tag{5.7}$$

and

$$\epsilon_T = 45\,(1 - r_{ma} - r_{qa})\,. \tag{5.8}$$

(U) From step 1 of our model it follows that r_{ma} may be zero. Then the polar diagram in Fig. 28 becomes trivial: the same distribution type is used for all aspect angles. If for a particular ship $\epsilon_s = 0$ (see (1) (b), (ii) and (iii) above), then we do not need L_d and W_d and the formulas (5.6)-(5.8) are replaced by

$$\epsilon_p = 90 r_{ma}\,, \tag{5.9}$$

$$\epsilon_T = 90\,(1 - r_{ma} - r_{qa})\,. \tag{5.10}$$

(U) To conclude the description of the proposed model for the variation of ship RCS fluctuations probability density at various aspect angles, we need to specify the density for the angle sector where the type is not "exact." According to our model (see (v) above), let $\sigma_{ma,t}$, $\sigma_{qa,t}$ be the RCS value according to the RCS fluctuation model at major aspect and quarter aspect angles, respectively. Then the RCS fluctuation model for the considered aspect region is

$$\sigma_t = \gamma\sigma_{ma,t} + (1 - \gamma)\sigma_{qa,t} \tag{5.11}$$

where γ is a function of aspect angle. We call this the mixed process model. In this model, $\sigma_{ma,t}$ and $\sigma_{qa,t}$ are considered independent processes and therefore the probability density function for RCS fluctuations according to this model is given by

$$p_T(\xi) = \frac{1}{\gamma}\int_0^{\frac{1}{1-\gamma}\xi} p_{ma}\left[\frac{1}{\gamma}\,\xi - \left(\frac{1}{\gamma} - 1\right)\sigma\right] p_{qa}(\sigma)\,d\sigma\,. \tag{5.12}$$

Here γ is a quadratic function of aspect angle as shown in Fig. 29.

(U) Obviously, other nonlinearities could have been chosen. The main idea is to provide for a transition section where the effects of the dominant scatterer (existing in the p_{ma} sector) are still visible but are fading rapidly as the aspect angle moves away from the p_{ma} sector. The quadratic variation is the simplest curve that will provide the desired behavior.

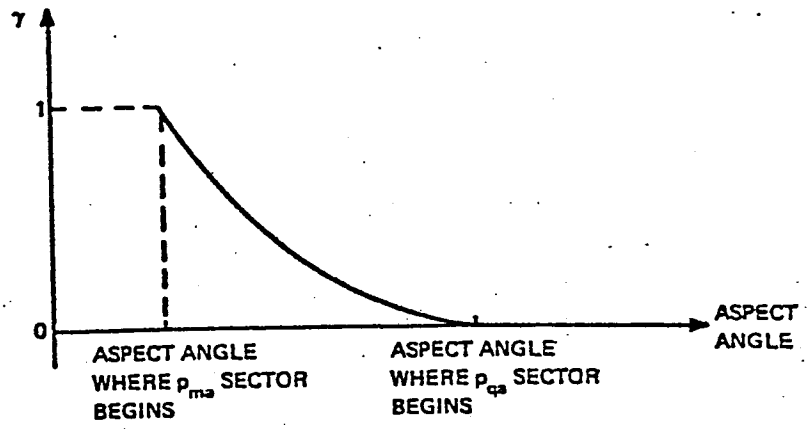

(U) Fig. 29—Illustrating variation of mixture parameter with aspect angle

6. GENERATION OF THE NECESSARY STOCHASTIC PROCESSES

(U) We have seen from section 2 that first-order statistics of RCS fluctuations can be of the following type: exponential (Rayleigh power), chi-square with four degrees of freedom, Rice power, and lognormal. From section 4, the autocovariance function of σ_t is a decaying exponential. These are the typical outcomes of experimental data processing. Our goal, as was explained at the end of section 2, is to generate a piecewise wide-sense stationary stochastic process with the above statistical properties. We have a serious constraint: the generation algorithm is called every pulse by the missile simulation package, so it must be fast. The form of the autocovariance function suggests first-order Gauss-Markov models. The non-Gaussian first-order statistics, however, require nonlinear transformations of the underlying Gauss-Markov models. In this section we provide the detailed descriptions of the stochastic process generation algorithms necessary for our model.

(U) We first give the algorithms that generate, to a very good approximation, a wide-sense stationary stochastic process with decaying exponential autocovariance function and with first-order statistics belonging to one of the four types mentioned in the beginning of the section.

6.1. Exponential (or Rayleigh-Power) Process

(U) Let $y_{1,t}$ and $y_{2,t}$ be two independent wide-sense stationary, zero-mean, Gaussian processes with identical autocovariance functions

$$E\{y_{1,t}y_{1,t+\tau}\} = E\{y_{2,t}y_{2,t+\tau}\} = R_y(\tau)$$

$$= R_g \exp(-\alpha\tau). \tag{6.1}$$

The processes $y_{1,t}$ and $y_{2,t}$ are very efficiently generated on the computer by the following first-order recursion:

$$y_{i,t+\Delta t} = Ay_{i,t} + Bw_t, \quad i = 1, 2, \tag{6.2}$$

where Δt is the basic time increment, which for us is the pulse-to-pulse time, and

$$\left.\begin{aligned} A &= \exp(-\alpha\Delta t)\,, \\ B &= \sqrt{R_g(1-A^2)}\,. \end{aligned}\right\} \tag{6.3}$$

The initialization of Eq. (6.2) is by a Gaussian random variable with mean zero and variance R_g. The stochastic process w_t is a Gaussian white noise (i.e., uncorrelated) with zero mean and variance 1. Efficient algorithms for generating Gaussian random variables can be found in Ref. 29, p. 104-113, and we have adopted the "polar method" ([29], p. 104).

(U) Let $R_g = 1$ and set

$$x_t = y_{1,t}^2 + y_{2,t}^2\,. \tag{6.4}$$

It is well known ([29], p. 120, exercise 16) that x_t has an exponential probability density with mean 2. If σ_m is the desired median, it follows from section 2 and in particular Eq. (2.10) that the random variable

$$\sigma_t = \frac{1.443\sigma_m}{2}\, x_t \tag{6.5}$$

has an exponential density with the desired median. We need to compute the autocovariance of the process σ_t. From Eq. (6.4), we have

$$E\{x_t\} = 2$$

and

$$E\{(x_t - E\{x_t\})(x_{t+\tau} - E\{x_{t+\tau}\})\} = E\{x_t x_{t+\tau}\} - 4\,. \tag{6.6}$$

Now

$$\begin{aligned} E\{x_t x_{t+\tau}\} &= E\{y_{1,t}^2 y_{1,t+\tau}^2\} + E\{y_{2,t}^2\}E\{y_{1,t+\tau}^2\} \\ &\quad + E\{y_{1,t}^2\}E\{y_{2,t+\tau}^2\} + E\{y_{2,t}^2 y_{2,t+\tau}^2\} \\ &= 2E\{y_{1,t}^2 y_{1,t+\tau}^2\} + 2\,, \end{aligned} \tag{6.7}$$

where we used the properties of the $y_{1,t}$ and $y_{2,t}$ processes. From appendix B, Eq. (B3), we have (see also Ref. 30, p. 264)

$$E\{y_{1,t}^2 y_{1,t+\tau}^2\} = 2R_y^2(\tau) + 1\,, \tag{6.8}$$

since we are using $R_g = 1$. From Eqs. (6.6-6.8) we obtain

$$E\{(x_t - E\{x_t\})(x_{t+\tau} - E\{x_{t+\tau}\})\} = 4R_y^2(\tau) = R_x(\tau)\,. \tag{6.9}$$

From Eqs. (6.5) and (6.9),

$$E\{\sigma_t\} = 1.443\sigma_m \,, \tag{6.10}$$

$$\begin{aligned} R_\sigma(\tau) &= E\{(\sigma_t - E\{\sigma_t\})(\sigma_{t+\tau} - E\{\sigma_{t+\tau}\})\} \\ &= (1.443\sigma_m)^2 R_y^2(\tau) \\ &= (1.443\sigma_m)^2 \exp(-2\alpha\tau) \,. \end{aligned} \tag{6.11}$$

From Eqs. (6.10) and (6.11), σ_t is wide-sense stationary. Moreover, since $y_{1,t}$ and $y_{2,t}$ obviously are ergodic (see Ref. 31, pp. 147–159 and in particular Ref. 32, pp. 20–21) and σ_t is a time invariant memoryless function of $y_{1,t}, y_{2,t}, \sigma_t$ is also ergodic. Finally, if t_c is the correlation time of the exponential process σ_t, we obtain, comparing Eq. (4.10) with Eq. (6.11),

$$\alpha = \frac{1}{2t_c} \,. \tag{6.12}$$

(U) Summarizing, in order to generate a wide-sense stationary process having exponential first-order density with given median σ_m and decaying exponential autocovariance function with given correlation time t_c, (a) compute α from Eq. (6.12), (b) construct two independent (0,1) Gaussian processes according to Eqs. (6.2–6.3), and (c) define σ_t via Eqs. (6.4–6.5).

6.2. Chi-Square With Four Degrees of Freedom Process

(U) Since ([29], p. 120, exercise 16) if x_1 and x_2 are two independent random variables with chi-square densities having ν_1 and ν_2 degrees of freedom, respectively, the random variable $x_3 = x_1 + x_2$ has a chi-square density with $\nu_1 + \nu_2$ degrees of freedom, this case is a direct application of the results in section 6.1. So we generate four independent Gaussian processes via Eqs. (6.2) and (6.3) with $R_g = 1$. Then

$$x_t = y_{1,t}^2 + y_{2,t}^2 + y_{3,t}^2 + y_{4,t}^2 \tag{6.13}$$

has a chi-square with four degrees-of-freedom density, with mean 4. So

$$\sigma_t = \frac{1.18}{4}\,\sigma_m x_t \tag{6.14}$$

has the same type density with the desired mean, as a result of Eq. (2.11). As for the autocovariance, it is easily computed, as in section 6.1:

$$E\{(x_t - E\{x_t\})(x_{t+\tau} - E\{x_{t+\tau}\})\} = 8R_y^2(\tau) = R_x(\tau) \tag{6.15}$$

and

$$\begin{aligned} R_\sigma(\tau) &= E\{(\sigma_t - E\{\sigma_t\})(\sigma_{t+\tau} - E\{\sigma_{t+\tau}\})\} \\ &= \frac{(1.18\sigma_m)^2}{2}\, R_y^2(\tau) = \frac{(1.18\sigma_m)^2}{2} \exp(-2\alpha\tau) \,. \end{aligned} \tag{6.16}$$

It is now easily established as before that σ_t is ergodic. Moreover, Eq. (6.12) is again valid.

(U) To summarize, the generation algorithm in this case consists of the following steps: (a) compute α from Eq. (6.12), (b) construct four independent (0,1) Gaussian processes according to Eqs. (6.2-6.3), and (c) define σ_t via Eqs. (6.13-6.14).

6.3. Lognormal Process

(U) Let y_t be a wide-sense stationary, zero-mean, Gaussian process with autocovariance given by Eq. (6.1). It is well known [13,29] that the random variable

$$x_t = \exp(y_t) \tag{6.17}$$

has a lognormal density (Eq. (2.9)) with median 1 and mean to median ratio $\exp(1/2R_g)$ (cf. Eq. (2.13)). Since, obviously, the mean to median ratio is invariant under scaling, the random variable

$$\sigma_t = \sigma_m x_t \tag{6.18}$$

has a lognormal density with median σ_m and the same mean to median ratio as x_t. Clearly,

$$E\{x_t\} = \exp(R_g/2), \tag{6.19}$$

and from well-known properties of the moment-generating function of vector Gaussian random variables ([30], p. 65) we obtain (see appendix B, Eq. (B4))

$$\begin{aligned} E\{x_t x_{t+\tau}\} &= E\{\exp(y_t + y_{t+\tau})\} \\ &= \exp[R_g + R_y(\tau)]. \end{aligned} \tag{6.20}$$

Therefore, the autocovariance of the σ_t process is

$$E\{(\sigma_t - E\{\sigma_t\})(\sigma_{t+\tau} - E\{\sigma_{t+\tau}\})\} = R_\sigma(\tau) = \sigma_m^2 \exp R_g [\exp R_y(\tau) - 1]. \tag{6.21}$$

It is easily seen from Eq. (6.21) that $R_\sigma(\tau) \geq 0$, $R_\sigma(\tau)$ is smooth, and $R_\sigma(\tau) \to 0$ as $\tau \to \infty$. Moreover, since

$$\frac{d}{d\tau} R_\sigma(\tau) = \sigma_m^2 \exp R_g \exp(R_g e^{-\alpha\tau})(-\alpha R_g) \exp(-\alpha\tau), \tag{6.22}$$

then $dR_\sigma(\tau)/d\tau < 0$ for all $\tau \geq 0$, and therefore $R_\sigma(\tau)$ is monotonically decreasing. Finally,

$$\frac{d^2R_\sigma(\tau)}{d\tau^2} = \sigma_m^2 \exp R_g \exp (R_g e^{-\alpha\tau})[\alpha^2 R_g^2 \exp (-2\alpha\tau)$$

$$+\alpha^2 R_g \exp (-\alpha\tau)] , \qquad (6.23)$$

that is,

$$\frac{d^2R_\sigma(\tau)}{d\tau^2} > 0 \quad \text{for all} \quad \tau \geq 0 .$$

From the above properties it is seen that $R_\sigma(\tau)$ resembles a decaying exponential, and this is supported by computations. In Fig. 30, various plots of $R_\sigma(\tau)$ are shown with $\sigma_m = 1$, $R_g = 1$, and $\alpha = 1, 0.5, 0.2, 0.1$, and 0.05. As a result of these computations, in order for $R_\sigma(\tau)$ (as given by Eq. (6.21)) to approximate the desired autocovariance (which is of the form (4.10)), the correlation time of $R_\sigma(\tau)$ (i.e., the time where $R_\sigma(\tau)$ falls to $1/e$ of its value for $\tau = 0$) is equated with the desired RCS fluctuations correlation time t_c. Thus

$$\exp R_g(e^{-\alpha t_c}) - 1 = \frac{1}{e} (\exp R_g - 1)$$

or

$$R_g \exp (-\alpha t_c) = \ln \left(1 + \frac{\exp R_g - 1}{e}\right)$$

$$\alpha = \frac{1}{t_c} \left\{ \ln R_g - \ln \left[\ln \left(1 + \frac{\exp R_g - 1}{e}\right)\right]\right\} . \qquad (6.24)$$

In Fig. 30 we also show the decaying exponential curves $\exp (-t/t_c)$, where t_c is computed from Eq. (6.24) for each value of α. The approximation is very good indeed. Of course, the value of t_c to be used in Eq. (6.24) is computed according to section 4. Again, since σ_t is a time-invariant, memoryless function of an ergodic process, it is also ergodic.

(U) To summarize, the algorithm for generating a lognormal process with an almost decaying exponential autocovariance function consists of the following steps: (a) given t_c and R_g, compute α from Eq. (6.24), (b) construct a $(0, R_g)$ Gaussian random process by first constructing a (0,1) Gaussian process according to Eqs. (6.2-6.3) and multiplying the result by $\sqrt{R_g}$, and (c) define σ_t via Eqs. (6.17-6.18). The parameters σ_m and R_g will be computed according to sections 2 and 3. As an additional useful fact, we observe that, usually, experiments provide the standard deviation of $10 \log_{10} \sigma_t$ in dB over m^2. Then

$$R_g = 0.53019 \text{ (standard deviation of } 10 \log_{10} \sigma_t \text{ in dB over } m^2)^2 . \qquad (6.25)$$

We also note that R_g corresponds to s^2 in Eq. (2.13).

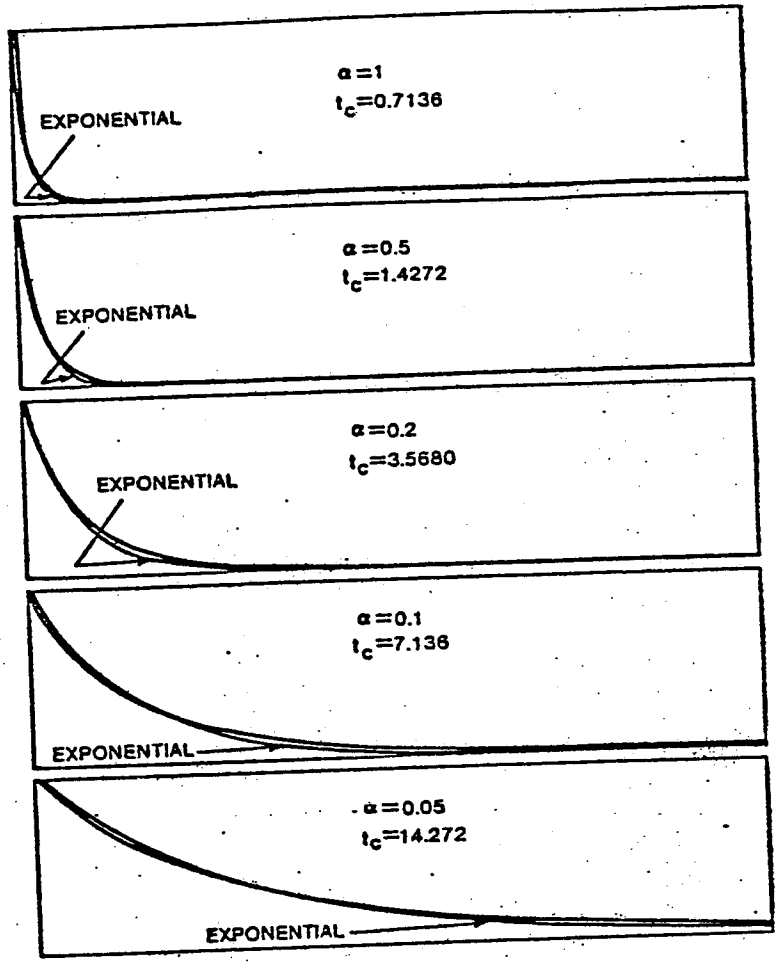

(U) Fig. 30—Comparing the autocovariance of the lognormal process (from Eq. (6.21) normalized so that $R_g(0) = 1$) with a decaying exponential (t_c is computed from α using Eq. (6.24))

6.4 Rice-Power Process

(U) Let $y_{1,t}$ and $y_{2,t}$ be as in section 6.1 (Eq. (6.1)). Define $x_{1,t}$, $x_{2,t}$ via

$$x_{1,t} = c + y_{1,t}$$
$$x_{2,t} = y_{2,t}. \tag{6.26}$$

If we let

$$x_t = \sqrt{x_{1,t}^2 + x_{2,t}^2}, \tag{6.27}$$

it is known that x_t has a Rice amplitude probability density (cf., Eq. (2.7) with $\alpha^2 = R_g$) ([30], pp. 150–167) (see also appendix B, Eq. (B5)). Therefore,

$$\sigma_t = x_t^2 \tag{6.28}$$

has a Rice-power probability density (see appendix B, Eq. (B9)). From Eqs. (6.26–6.28),

$$\sigma_t = (c + y_{1,t})^2 + y_{2,t}^2$$

$$= R_g \left[\left(\frac{c}{\sqrt{R_g}} + \frac{y_{1,t}}{\sqrt{R_g}} \right)^2 + \left(\frac{y_{2,t}}{\sqrt{R_g}} \right)^2 \right]. \tag{6.29}$$

Let

$$z_{1,t} = \frac{y_{1,t}}{\sqrt{R_g}}$$

$$z_{2,t} = \frac{y_{2,t}}{\sqrt{R_g}}. \tag{6.30}$$

Then $z_{1,t}$ and $z_{2,t}$ are wide-sense stationary Gaussian random processes with mean zero and autocovariance $R_z(\tau) = \exp(-\alpha\tau)$, and $c/\sqrt{R_g} = \sqrt{2}m$. Therefore, if we use the expression (see Eq. (B8) from appendix B)

$$\bar{\sigma} = R_g(1 + m^2)$$

then the process

$$\sigma_t = \frac{\bar{\sigma}}{2(1+m^2)} \left[(\sqrt{2}m + z_{1,t})^2 + z_{2,t}^2 \right] \tag{6.31}$$

has the desired probability density. To introduce the median in Eq. (6.31), we use the results of appendix A, where the mean to median ratio is computed as a function of m^2 (Table A1 and Fig. A1). So finally

$$\sigma_t = \rho(m^2) \frac{1}{2(1+m^2)} \sigma_m \left[(\sqrt{2}m + z_{1,t})^2 + z_{2,t}^2 \right]. \tag{6.32}$$

For the autocovariance function we have

$$E\{(\sigma_t - E\{\sigma_t\})(\sigma_{t+\tau} - E\{\sigma_{t+\tau}\})\}$$

$$= E\{\sigma_t \sigma_{t+\tau}\} - \bar{\sigma}^2$$

$$= \frac{\bar{\sigma}^2}{4(1+m^2)^2} E\left\{ \left[(\sqrt{2}m + z_{1,t})^2 + z_{2,t}^2 \right] \left[(\sqrt{2}m + z_{1,t+\tau})^2 + z_{2,t+\tau}^2 \right] \right\}$$

$$- \bar{\sigma}^2 . \tag{6.33}$$

Using

$$E\{z_{1,t}^2 z_{1,t+\tau}^2\} = 2R_z^2(\tau) + R_z^2(0)$$

(Eq. (B3), derived in the result of appendix B), we compute the indicated expectation, which equals

$$\begin{aligned}
&E\{z_{1,t}^2 z_{1,t+\tau}^2\} + 2\sqrt{2}mE\{z_{1,t}z_{1,t+\tau}^2\} + 2m^2E\{z_{1,t+\tau}^2\} \\
&+E\{z_{2,t}^2\}E\{z_{1,t+\tau}^2\} + 2\sqrt{2}mE\{z_{1,t}^2 z_{1,t+\tau}\} \\
&+8m^2E\{z_{1,t}z_{1,t+\tau}\} + 4\sqrt{2}m^3E\{z_{1,t+\tau}\} \\
&+2\sqrt{2}mE\{z_{2,t}^2\}E\{z_{1,t+\tau}\} + 2m^2E\{z_{1,t}^2\} + 4\sqrt{2}m^2E\{z_{1,t}\} \\
&+4m^4 + 2m^2E\{z_{2,t+\tau}^2\} + E\{z_{1,t}^2 z_{2,t+\tau}^2\} \\
&+2\sqrt{2}mE\{z_{1,t}\}E\{z_{2,t+\tau}^2\} + 2m^2E\{z_{2,t+\tau}^2\} + E\{z_{2,t}^2 z_{2,t+\tau}^2\} \\
&= 2\left[2R_z^2(\tau) + R_z^2(0)\right] + 4m^4 + 8m^2 + 2 + 8m^2R_z(\tau). \qquad (6.34)
\end{aligned}$$

Using Eq. (6.34) in Eq. (6.33), we obtain

$$\begin{aligned}
R_\sigma(\tau) &= \frac{\bar{\sigma}^2}{4(1+m^2)^2}\left[4(m^2+1)^2 + 4R_z^2(\tau) + 8m^2R_z(\tau)\right] - \bar{\sigma}^2 \\
&= \frac{\bar{\sigma}^2}{(1+m^2)^2}\left[\exp(-2\alpha\tau) + 2m^2\exp(-\alpha\tau)\right]. \qquad (6.35)
\end{aligned}$$

It thus follows that σ_t is wide-sense stationary, and because $z_{1,t}, z_{2,t}$ are ergodic and σ_t is (via Eq. (6.31)) a time-invariant memoryless function of ergodic processes, it is also ergodic.

(U) To compare $R_\sigma(\tau)$ with a decaying exponential, we normalize so that $R_\sigma(0) = 1$. So

$$\frac{R_\sigma(\tau)}{R_\sigma(0)} = \frac{1}{1+2m^2}\exp(-2\alpha\tau) + \frac{2m^2}{1+2m^2}\exp(-\alpha\tau). \qquad (6.36)$$

Since this function is a convex combination of two decaying exponentials, it can be very well approximated by a decaying exponential if we match the correlation times. Indeed, for small values of m^2, Eq. (6.36) is very well approximated by $\exp(-2\alpha\tau)$, while for large values of m^2 it reduces to $\exp(-\alpha\tau)$. So we obtain the relation between α and t_c via

$$\begin{aligned}
&\frac{\exp(-2\alpha t_c) + 2m^2(\exp - \alpha t_c)}{1+2m^2} = \frac{1}{e}, \\
&\exp(-\alpha t_c) = -m^2 + \sqrt{m^4 + \frac{1+2m^2}{e}}, \qquad (6.37)
\end{aligned}$$

Continued

$$\alpha = -\frac{1}{t_c} \ln \left(-m^2 + \sqrt{m^4 + \frac{1 + 2m^2}{e}} \right). \tag{6.37}$$

These considerations are supported with the results of computations, comparing the normalized autocovariance function (6.36), with α obtained through Eq. (6.37), with the single decaying exponential $\exp(-t/t_c)$, as shown in Fig. 31. The approximation is excellent.

(U) To summarize, the algorithm for generating a Rice-power process with an almost decaying exponential autocovariance function consists of the following steps: (a) given t_c and m^2, compute α from Eq. (6.37), (b) construct two (0,1) Gaussian random processes $z_{1,t}, z_{2,t}$ according to Eqs. (6.2-6.3), (c) given m^2, compute $\rho(m^2)$ from Fig. A1, and (d) given σ_m, define σ_t via Eq. (6.32). The parameters σ_m and m^2 will be computed according to sections 2 and 3.

(U) This concludes the description of the algorithms generating wide-sense stationary stochastic processes with decaying exponential autocovariance function and first-order statistics of the desired type. These are all incorporated in the subroutines RAPR1-RAPR4.

6.5. Model Completion

(U) Several remarks are now in order. First observe that we succeeded in providing algorithms that use at most four first-order linear Gauss-Markov models followed by memoryless nonlinearities. This approach makes our algorithms very fast compared to other algorithms (see Ref. 33, ch. 8), for example, those based on independence of spectral samples which use a much larger number of simple random process generators [33]. As we explained in the beginning of this section, the development of fast algorithms was an essential constraint for the simulation model. Next, notice that the proposed model specifies all finite-order statistics of the generated stochastic process, since we essentially give a dynamic system realization of the process. The model matches the first- and second-order statistics as derived from experimental data. This, recall, was our goal (see section 2). It will be interesting to test whether the higher order statistics, as generated by the model, are in agreement with experimental data. For the latter, however, new data bases have to be created. In view of the total reliance of radar design and evaluation methods on second-order statistics, the value of such an investigation toward improved quality of simulation is doubtful.

(U) We now proceed to describe the necessary algorithms for the completion of the model. To make the model piecewise wide-sense stationary, the parameters of the stochastic process generation algorithms should all be updated at the same time, and at appropriate intervals. These parameters are the correlation time t_c, the median RCS (for exponential and chi-square with four degrees of freedom), and in addition, the mean to median ratio (for lognormal) or m^2 (for Rice power). As we noted in sections 2 and 3, the two latter parameters can be deduced from the variance of RCS fluctuations. Since, from sections 3 and 4, the major factor in the variation of these parameters *for ships* is the variation of aspect angle, we update all these parameters whenever a change in aspect angle of a predetermined size has occurred (we currently use 2°). The parameters remain constant between these changes. This, obviously, makes the model piecewise wide-sense stationary.

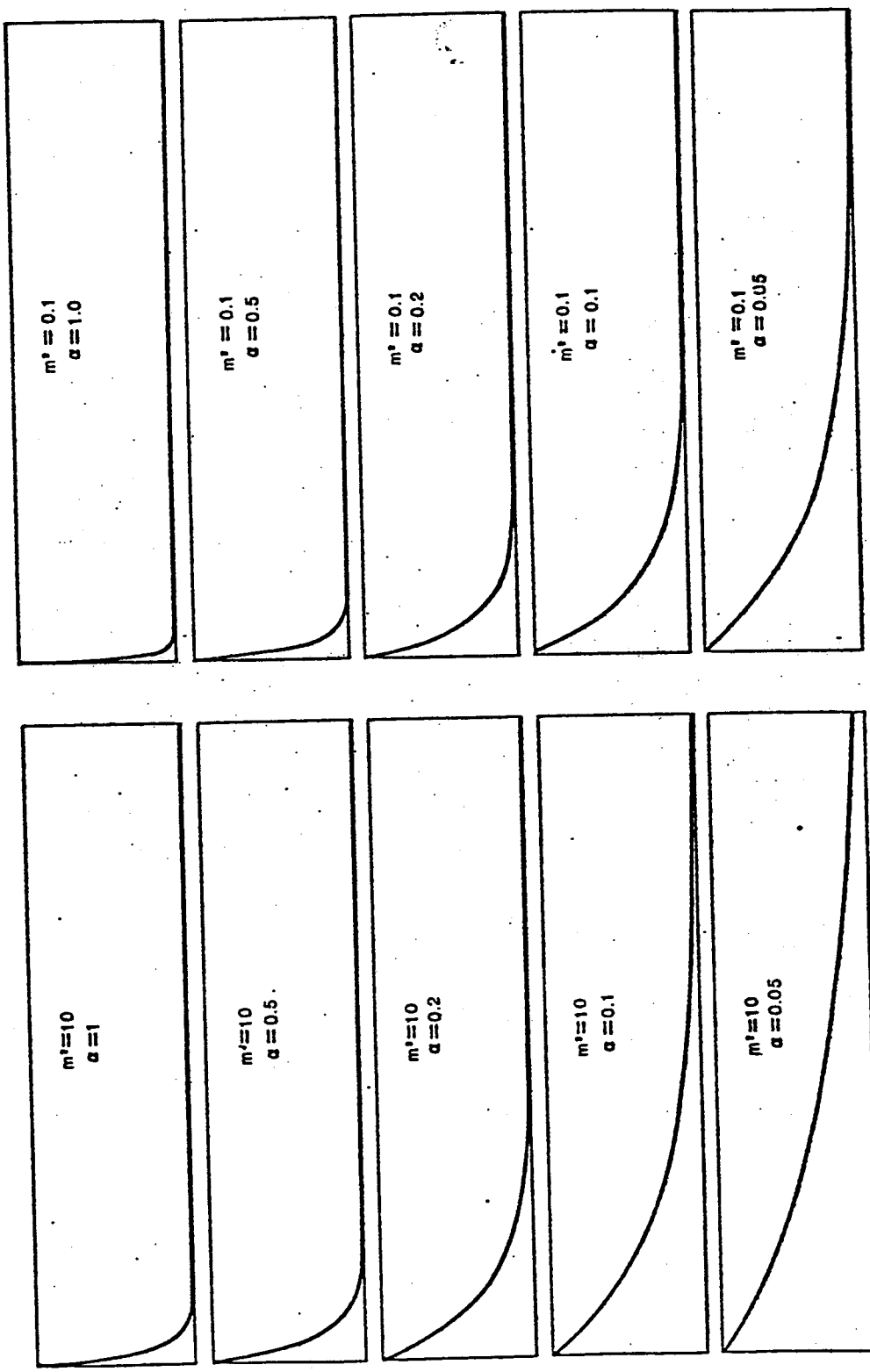
m' = 0.1
α = 1.0
m' = 0.1
α = 0.5
m' = 0.1
α = 0.2
m' = 0.1
α = 0.1
m' = 0.1
α = 0.05
m'=10
α =1
m'=10
α = 0.5
m'=10
α =0.2
m'=10
α =0.1
m'=10
α =0.05

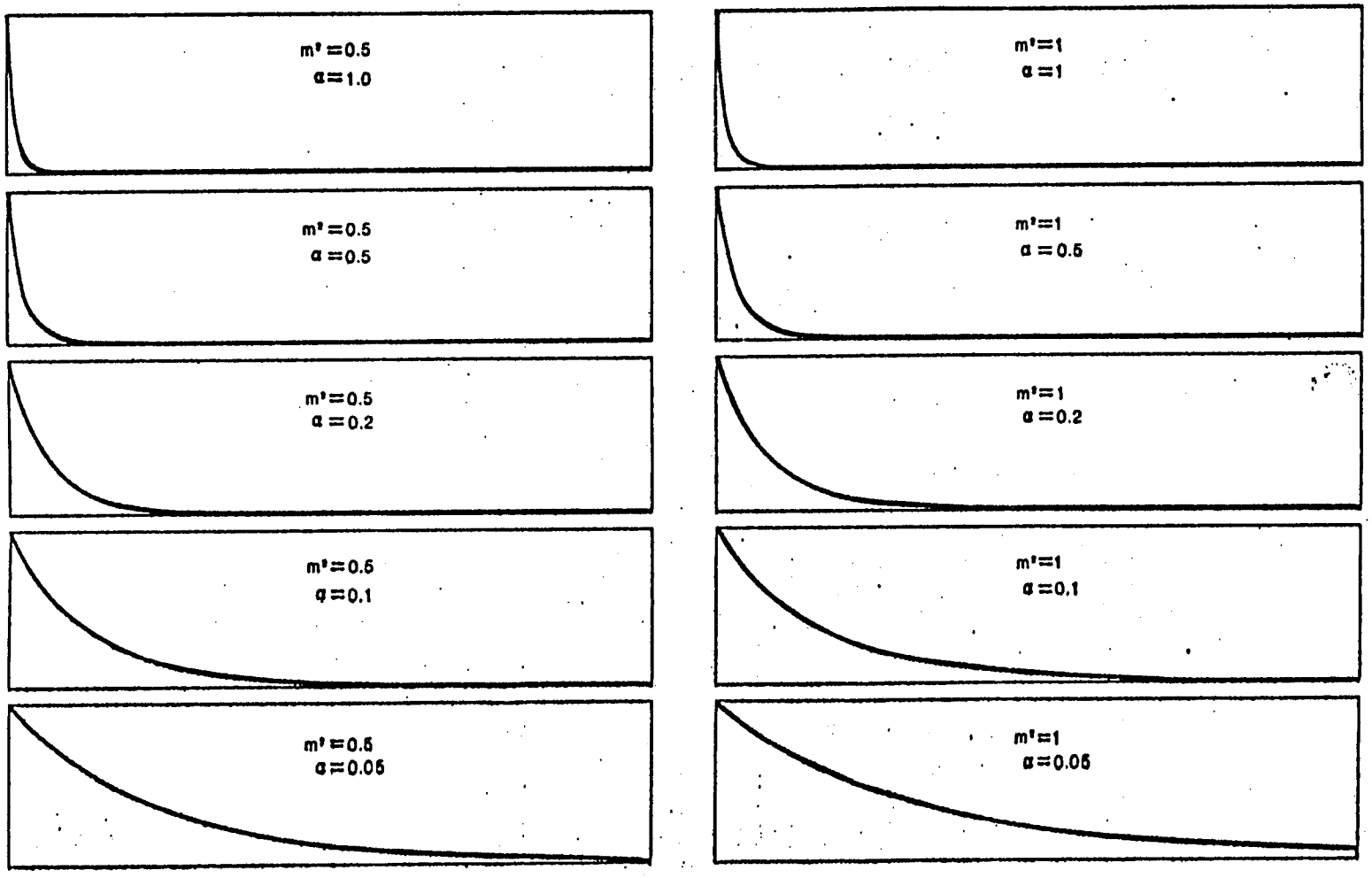

(U) Fig. 31—Comparing the normalized autocovariance (Eq. (6.36)) with a decaying exponential. In most cases, the two curves are so close that they cannot be distinguished.

(U) We recall from section 5 (cf. (v.) and Eq. (5.11)) that there are aspect angle sectors where a mixed process (e.g., Eq. (5.11)) is required by the model. Therefore, a different random process generation algorithm is required for these cases. An algorithm which consists of a minor modification of the above four basic algorithms is highly desirable due to considerations of complexity and computation time of the overall model. Fortunately, the algorithm for the mixed process is straightforward:

(a) generate two independent, wide-sense stationary stochastic processes, with decaying exponential autocovariance function $\sigma_{1,t}$ and $\sigma_{2,t}$ and first-order probability density p_{ma} and p_{qa}, respectively, employing the appropriate algorithms in sections 6.1-6.4.

(b) given the mixture parameter $\gamma \in [0,1]$, set

$$\sigma_t = \gamma\sigma_{1,t} + (1-\gamma)\sigma_{2,t}\,. \tag{6.38}$$

Then the first-order density function of the random process is given by Eq. (5.13). For the autocovariance, let $\bar{\sigma}_1$ and $\bar{\sigma}_2$ be the constant means and $R_{\sigma_1}(\tau)$ and $R_{\sigma_2}(\tau)$ the autocovariances of $\sigma_{1,t}$ and $\sigma_{2,t}$. By the independence of $\sigma_{1,t}$ and $\sigma_{2,t}$

$$\bar{\sigma} = E\{\sigma_t\} = \gamma\bar{\sigma}_1 + (1-\gamma)\bar{\sigma}_2 \tag{6.39}$$

$$\begin{aligned} R_\sigma(\tau) &= E\{\sigma_t\sigma_{t+\tau}\} - \bar{\sigma}^2 \\ &= \gamma^2 R_{\sigma_1}(\tau) + (1-\gamma)^2 R_{\sigma_2}(\tau)\,. \end{aligned} \tag{6.40}$$

From Eqs. (6.39) and (6.40), the new process σ_t is also wide-sense stationary. Since, as we noted in sections 6.1-6.4, $\sigma_{1,t}$ and $\sigma_{2,t}$ are ergodic, and σ_t is a time-invariant memoryless function of ergodic process, it is also ergodic. So the use of time averages for valid t in this portion of the model is also justified.

(U) By construction, $R_{\sigma_1}(\tau)$ and $R_{\sigma_2}(\tau)$ are decaying exponentials. Since we want $R_\sigma(\tau)$ to be also a decaying exponential, we must construct in (a) (above) $\sigma_{1,t}$ and $\sigma_{2,t}$ to have the same correlation time t_c. Then

$$\begin{aligned} R_{\sigma_1}(\tau) &= R_1 \exp(-\tau/t_c)\,, \\ R_{\sigma_2}(\tau) &= R_2 \exp(-\tau/t_c)\,, \end{aligned} \tag{6.41}$$

and therefore

$$R_\sigma(\tau) = \left[\gamma^2 R_1 + (1-\gamma)^2 R_2\right]\exp(-\tau/t_c)\,. \tag{6.42}$$

That is, σ_t will have an autocovariance function of the desired form. It is important to realize that $\bar{\sigma}_1 \neq \bar{\sigma}_2$ and $R_1 \neq R_2$, since the two underlying processes will have different mean to median ratios (due to their different types) and different variances (e.g., $\sigma_{1,t}$ being lognormal, $\sigma_{2,t}$ being exponential). To complete this part of the algorithm we must choose R_1 and R_2 approximately (recall that the variation of γ is described at the end of section 5). This will be required *only* in cases where the corresponding probability

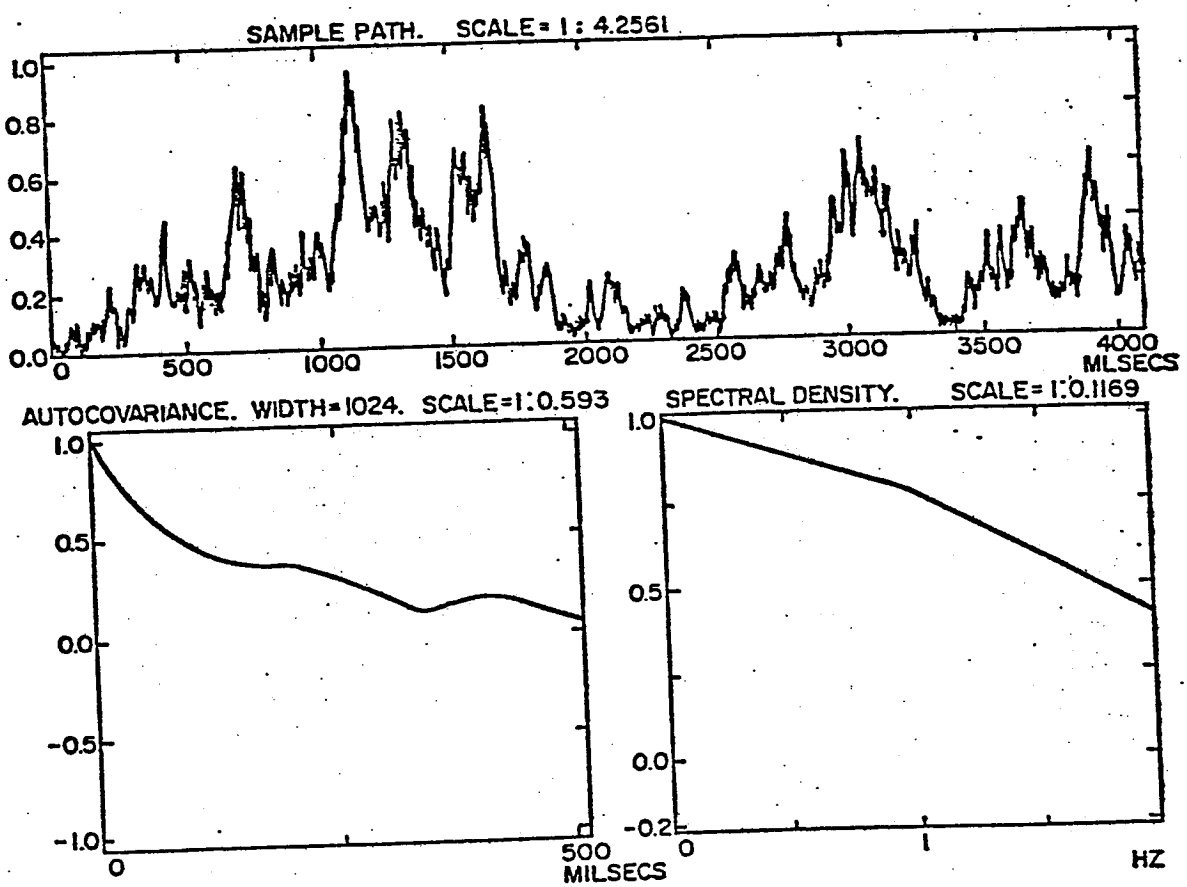

(U) Fig. 33—Output from the chi-square process generator. t_c = 0.100 s, interpulse time = 0.0005 s, median RCS = 1 m^2.

density has two parameters (i.e., it is lognormal or Rice power). In such cases, the appropriate value for R_1 or R_2 will be selected according to our discussion in sections 2 and 3. To be consistent with our piecewise wide-sense stationary approximation, the mixture parameter γ is updated at the same time as the other parameters (i.e., every time interval that a change in aspect angle of 2° has occurred). The mixed process model is in subroutine RAPR5. The selection of the appropriate stochastic process generator, including the mixed process, is performed by the subroutine TARDEN.

(U) The final point of this section concerns the reduction of random-number generators needed and the procedures for safeguarding their independence, as called for by the analysis underlying the model. The method employed to resolve these questions will have important consequences on the overall complexity and quality of implementation (i.e., coding) of the proposed model. Recall that we need to generate per ship, in the simulation scenario, up to four independent Gaussian (0,1) processes with decaying exponential autocovariance functions: one for lognormal, two for exponential, two for Rice power, and four for chi-square with four degrees of freedom. The Gaussian processes used for different ships must be independent. The employed "polar method" ([29], p. 104) for generating Gaussian random variables requires two independent random-number generators and generates two independent (0,1) Gaussian random variables. Therefore, a "naive" implementation will require eighteen independent random-number generators and nine arrays per ship to store the Gaussian processes. Using the redundancy of Gaussian random variables generated by pairs of random-number generators (see "polar method" ([29], p. 104)), we can reduce the requirements to ten independent random-number generators and nine memory arrays per ship. In addition to introducing an undesirable increase in the complexity and size of the simulation code (and necessary memory), this "naive" approach to these problems creates severe bookkeeping problems for the switching from one stochastic process generator to another, and raises serious questions about the smoothness of the parameter updating procedure. Moreover, since all independent random-number generators will be implemented via random initialization of the basic random generator resident in the computer system, large numbers of random-number generators are undesirable since their independence can be severely impaired. Our solution to these problems relies on the fact that the model needs at most four independent Gaussian processes for aspect angle regions with fixed density and six for aspect angle regions with mixed density. The value of σ_t is given at any time by an appropriate nonlinear function of the values of these underlying Gaussian processes. Therefore, we need to run at most six independent Gaussian process generators. Employing a random shuffling algorithm (Ref. 29, p. 125), we can generate the necessary six random numbers employing only two random-number generators per ship. Moreover, we only run the number of Gaussian process generators necessary in each case (depending on aspect angle), the rest remaining idle. At time instances where the crossing of the boundary between aspect angle sectors with different probability density types (see Fig. 28) requires switching to a different stochastic process generator, the appropriate initializations of the Gaussian arrays are performed by the subroutine DNINTF. This subroutine utilizes the final values of the Gaussian arrays from the previous aspect sector, and if necessary creates additional Gaussian (0,1) random variables, to provide the necessary number of (0,1) Gaussian random variables to initialize the process generator for the new aspect-angle sector. Therefore, our solution requires two independent random-number generators and six memory arrays per ship (a considerable reduction from ten and nine), and employs a very simple interfacing procedure.

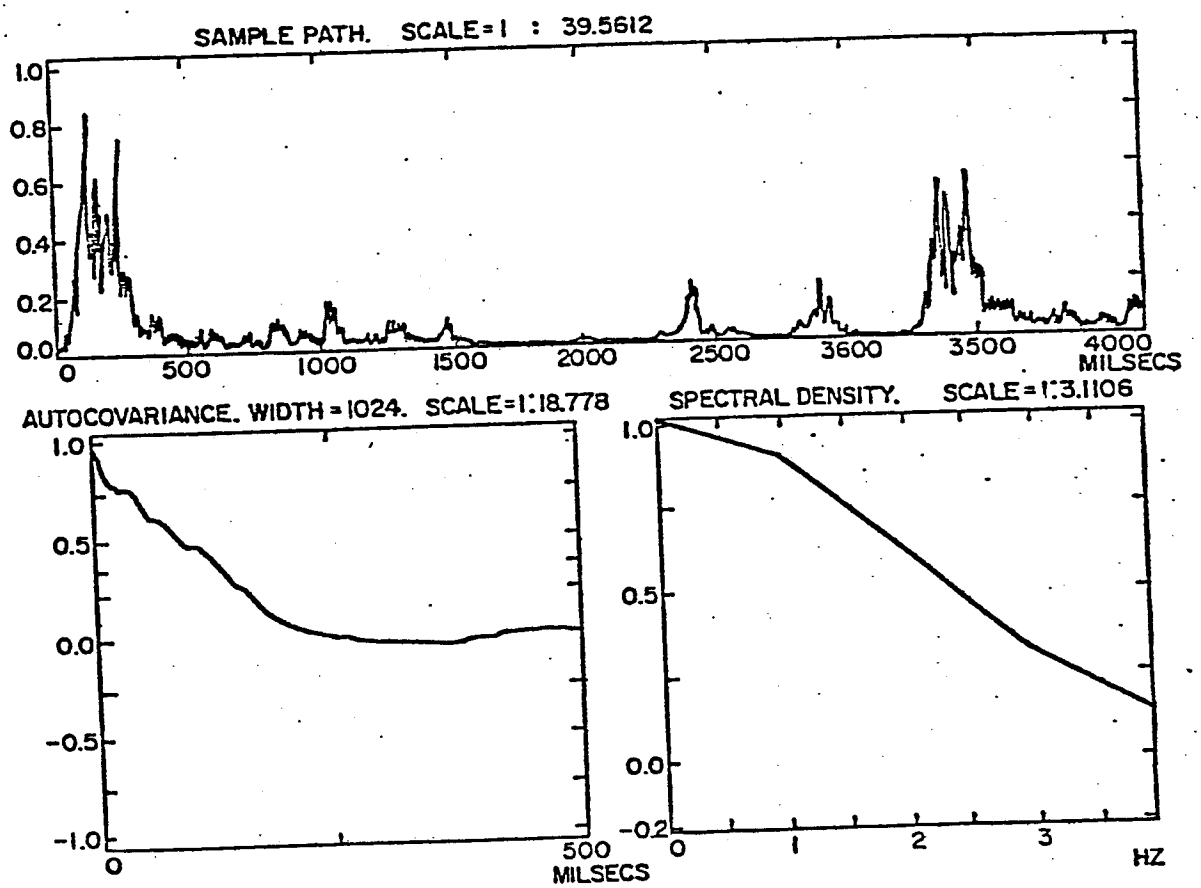

(U) Fig. 34—Output from the lognormal process generator. t_c = 0.100 s, interpulse time = 0.0005 s, median RCS = 1 m^2, mean-to-median ratio = 2.00.

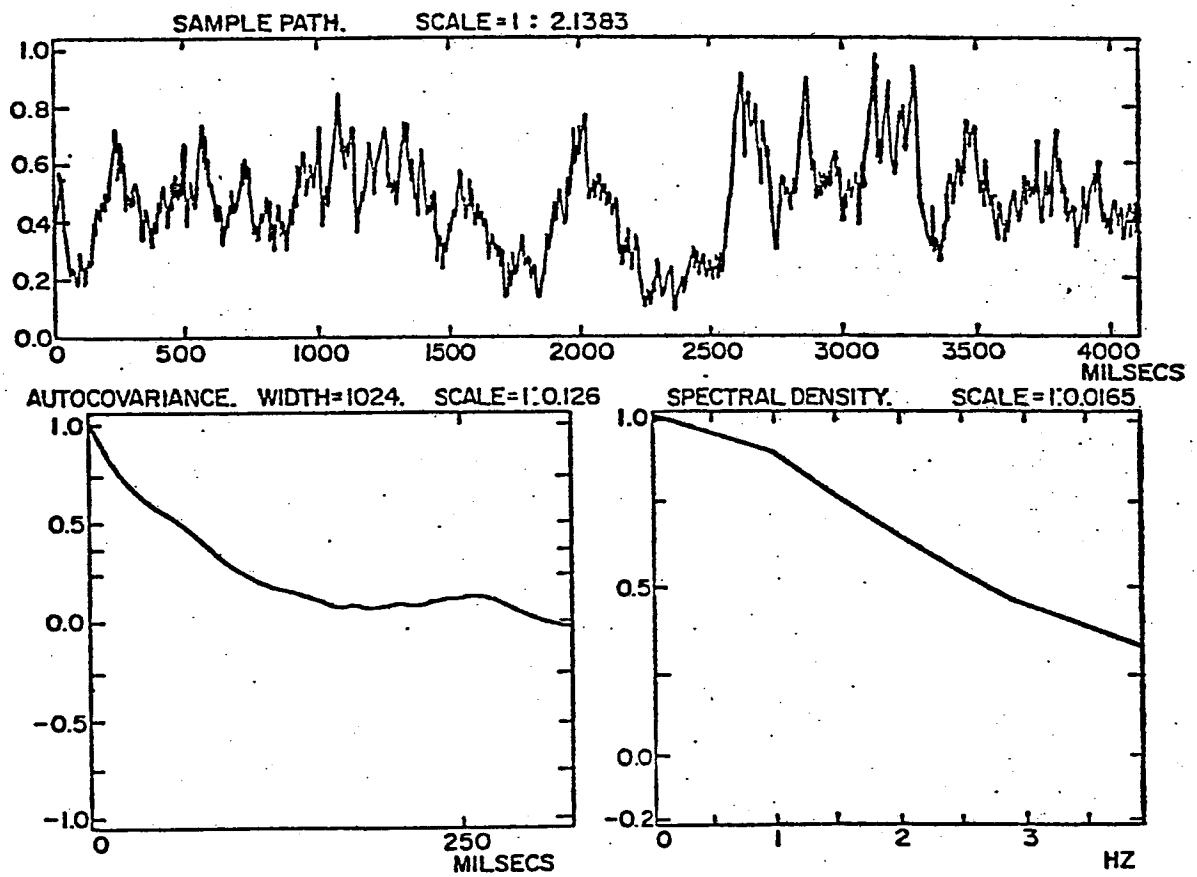

(U) Fig. 35—Output from the Rice-power process generator. t_c = 0.100 s, interpulse time = 0.0005 s, median RCS = 1 m^2, ratio of steady power to average random power = 10.00.

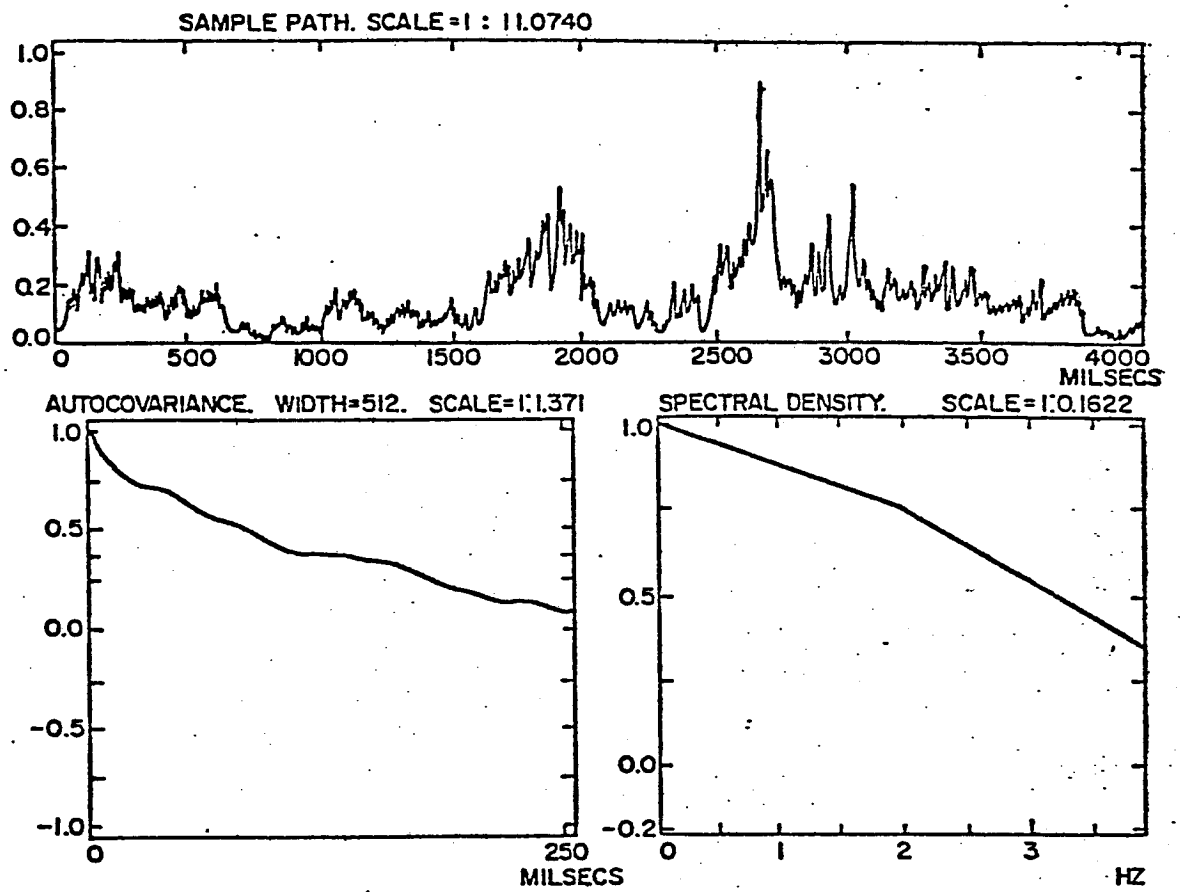

(U) Fig. 36—Output from the mixed process generator (here, exponential and lognormal). $t_c = 0.100$ s, interpulse time = 0.0005 s, median RCS = 1 m^2, mean-to-median ratio 1.8, $\gamma = 0.5$.

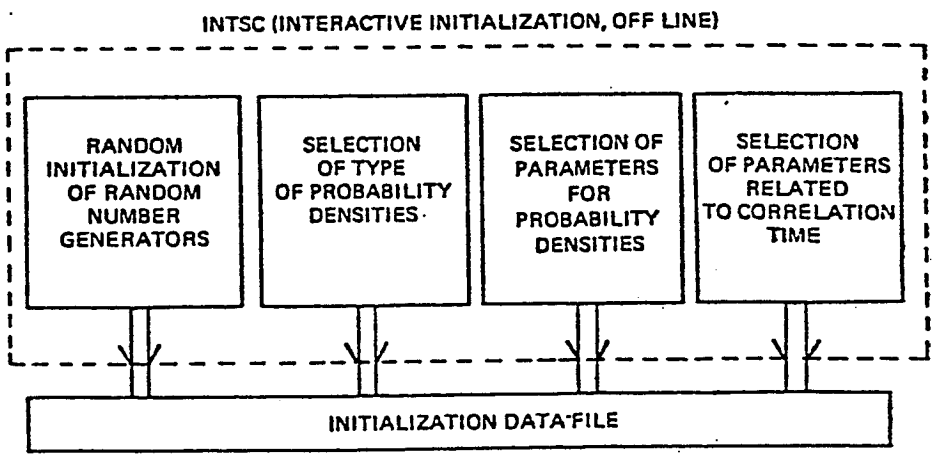

(U) Fig. 37—Flow chart for initialization program

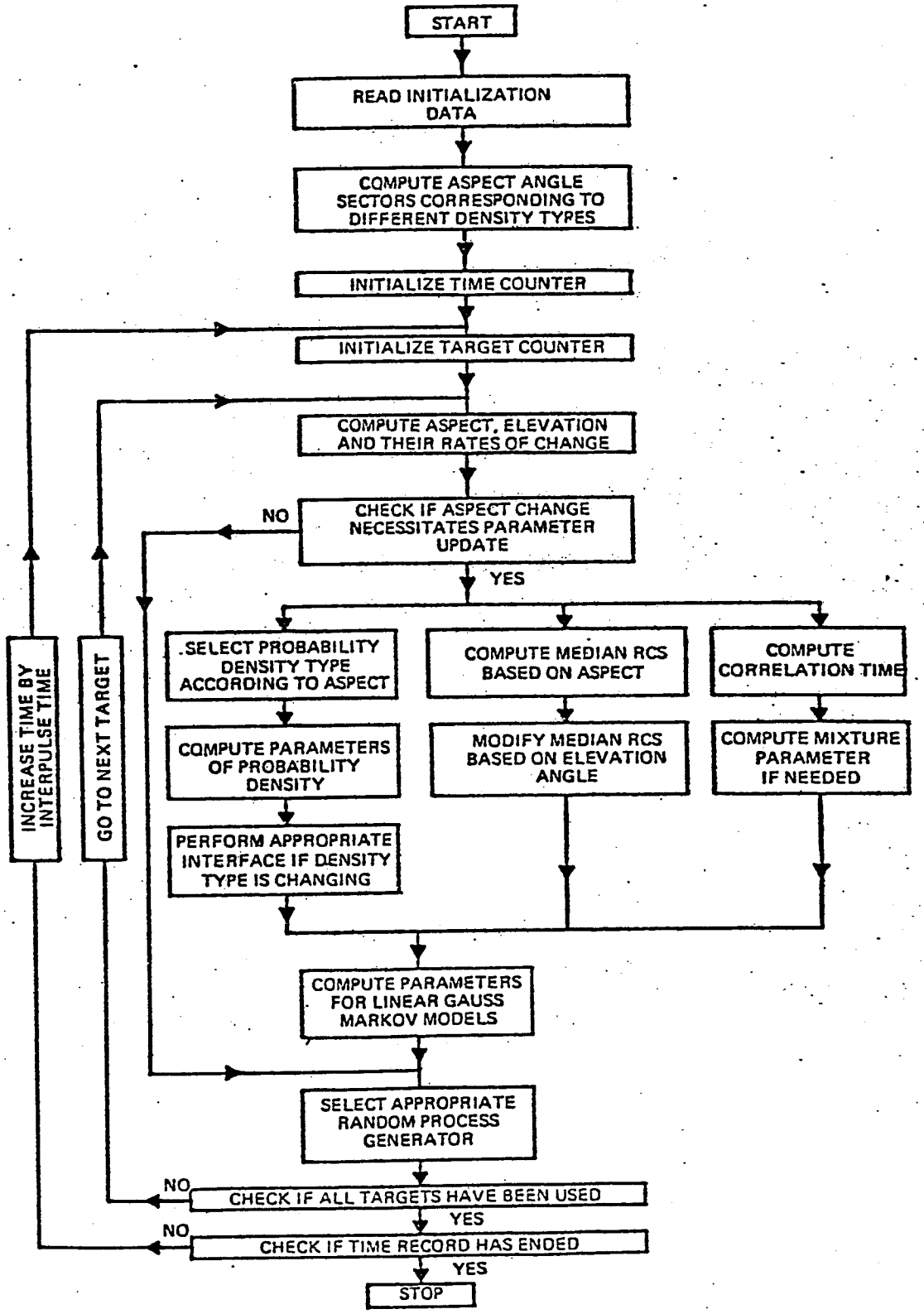

(U) Fig. 38—Comprehensive flowchart of RCS scintillation program

(U) From the description of the model, it should be apparent that several parameters are required as input for a particular simulation scenario. To facilitate initialization and to guarantee a systematic way for inputing all of the required parameters in the model, initialization is done off-line and prior to executing the main scintillation program SCINT 2. This is achieved by the interactive program INTSC, which automatically requests appropriate input from the user, provides necessary sources, displays appropriate charts, and outputs the selected values to a data file, after the user has selected the appropriate values for the parameters and is satisfied with the various diagnostic charts. This data file serves then as input file to the main program SCINT 2. The functions performed by INTSC are summarized below (see Fig. 37).

(a) Generate pairs of integers which are used for initialization of the random-number generators required in the model (two per ship). For obvious reasons, this is done in a random fashion tied to the time of day the program is called.

(b) Select, as described in section 5, the probability densities for each ship at major aspect and quarter aspect angles. Input the percentage of densities that are to be of each of these two types according to section 5. Input values for the characteristic length L_d and characteristic width W_d (see section 5).

(c) Select one of the two models for variation of median RCS as function of aspect angle (see section 3). Input values for median RCS at the bow if a depression at the bow is desired (see section 3). This is done for each ship.

(d) Input values for the ship's hull height as a function of aspect angle; quantize to ten distinct values at most. Input values for the depression angle where an increase in median is observed (see section 3). Input values for the constant used in the elevation dependence of median RCS (see section 3) as function of aspect angle; quantize to ten distinct values at most. This is done for each ship.

(e) If lognormal or Rice power is selected in (b) above, input values for the mean to median ratio (for lognormal) or ratio of steady power to average random power (for Rice) as functions of aspect angle; quantize to ten and twenty distinct values at most, respectively. This is also done for each ship.

(f) Input, for each ship, values for average random rate of change of aspect angle, elevation angle, ship's pitch, ship's roll, and rms pitch and roll angles, according to section 4.

ACKNOWLEDGMENTS

(U) I thank J. Lawrence for many stimulating discussions on this subject and R. Alvestad for help with the computations related to this report.

REFERENCES

1. T.J. Consroe, "Analysis of Centroid Decoying Against a Specific Electromagnetic Threat System," *NRL Report 7515* (Jan. 1973). (Secret Report, Unclassified Title.)

2. "Description of Angle ECM Simulation for Over Water Paths," Riverside Research Institute, Final Rpt. F/346-7-10, Dec. 1975. (Secret Report, Unclassified Title.)

3. R. Conklin, "Final Report for DARPA ANTRAC Field Test Evaluation—Phase A (U)," Norden Secret Report 1255-R-0002 (Mar. 1976).

4. F.E. Nathanson, *Radar Design Principles*, McGraw-Hill, New York, 1969.

5. D.K. Barton, *Radar System Analysis*, Prentice-Hall, Englewood Cliffs, 1964.

6. M.I. Skolnik, *Introduction to Radar Systems*, McGraw-Hill, New York, 1962.

7. M.I. Skolnik, ed. *Radar Handbook*, McGraw-Hill, New York, 1970.

8. W. Earl Hall, Jr., "System Identification—An Overview," *Naval Research Reviews*, pp. 1–20 (Apr. 1977).

9. K.J. Åström and P. Eykhoff, "System Identification—A Survey," *Automatica*, 7, pp. 123–162 (1971).

10. P. Eykhoff, *System Identification, Parameter and State Estimation*, Wiley, New York, 1974.

11. John S. Baras, "Sea Clutter and Angle Noise Simulation," NRL Report, to appear.

12. John S. Baras, "Multipath Effects Simulation," NRL Report, to appear.

13. A. Papoulis, *Probability, Random Variables, and Stochastic Processes*, McGraw-Hill, New York, 1965.

14. P. Beckmann and A. Spizzichino, *The Scattering of Electromagnetic Waves from Rough Surfaces*, Pergamon Press, New York, 1963.

15. P. Swerling, "Probability of Detection for Fluctuating Targets," Rand Corporation, RM-1217, March 17, 1954.

16. P. Swerling, "Probability of Detection for Some Additional Fluctuating Target Cases," Aerospace Corp. Rept. TOR-669 (9990) -14, El Segundo, California, Mar. 1966.

17. G.R. Heidbreder and R.L. Mitchell, "Detection Probabilities for Log-Normally Distributed Signals," *IEEE Trans.* on Aerospace and Electronic Systems, AES-3, (1) pp. 5–13 (Jan. 1967).

18. P.H.R. Scholefield, "Statistical Aspects of Ideal Radar Targets," *Proc. IEEE* 55, (4) pp. 587–89 (Apr. 1967).

19. J.F. Diggs, J.A. Burkett, J.C. Daley, W.T. Davis, and J.T. Ransone, Jr., "Radar Cross-Section Studies of Ships," NRL Report 7141 (Jan. 21, 1971). (Confidential)

20. F.L. Beckner, C.Z. Crow, C.R. Griffin, and D.K. Ingram, "*L*-Band Ship Echo Range Profiles for 50 and 100 Ft. Range Resolutions," Technical Report, Univ. of Texas at Austin, ARL-TR-74-49, Oct. 25, 1974.

21. F.L. Beckner, R.R. Kelly, III, W.S. Olsen, and T.F. Stipulkosky, "Frequency Agility, Fixed Frequency, and High Range Resolution Measurements of Ship Target and Sea Clutter Echoes at *L*-Band," Technical Report, Univ. of Texas at Austin, ARL-TR-70-1, Jan. 2, 1970. (Secret Report, Unclassified Title.)

22. F.L. Beckner, C.Z. Crow, and D.K. Ingram, "A Study of *L*-Band Ship Echo Data at Various Depression Angles, Aspect Angles, and Range Resolutions," Technical Report Univ. of Texas at Austin ARL-TR-74-43, Oct. 16, 1974. (Secret Report, Unclassified Title.)

23. F.L. Beckner, "Final Report on Phase 1, N123 (62738) 52022A(X), Covering the Period 23 December 1964–30 November 1965," Technical Report GP-4, FLD/GP 17, 17/9, Jan. 18, 1966. (Confidential Report, Unclassified Title.)

24. H.A. Corriher, Jr., Berry O. Pyron, R.D. Wetherington, and A.B. Abeling, "Radar Reflectivity of Sea Targets, Volume I," Technical Report, Georgia Institute of Technology, 1968.

25. S.O. Rice, "Statistical Properties of a Sine Wave Plus Random Noise," *Bell System Technical Journal* 27, pp. 109–157 (Jan. 1948).

26. K.A. Norton, L.E. Vogler, W.V. Mansfield, and P.J. Short, "The Probability Distribution of the Amplitude of a Constant Vector Plus a Rayleigh-Distributed Vector," *Proc. I.R.E.* 43, pp. 1354–1361 (1955).

27. M.W. Long, *Radar Reflectivity of Land and Sea*, Lexington Books, Lexington, Mass., 1975.

28. D.E. Kerr (Editor), *Propagation of Short Radio Waves*, McGraw-Hill, New York, 1951.

29. D.E. Knuth, *The Art of Computer Programming*, 2nd. ed., Vol. 2, Addison-Wesley, Reading, Mass. 1969.

30. J.B. Thomas, *An Introduction to Statistical Communication Theory*, Wiley, New York, 1969.

31. H. Cramer and M.R. Leadbetter, *Stationary and Related Stochastic Processes*, Wiley, New York, 1967.

32. A.M. Yaglom, *An Introduction to the Theory of Stationary Random Functions*, Prentice-Hall Inc., Englewood Cliffs, N.J. 1962.

33. R.L. Mitchell, *Radar Signal Simulation*, Artech House, Inc., Dedham, Mass., 1976.

34. M. Abramowitz and I.A. Stegun, *Handbook of Mathematical Functions*, AMS55, National Bureau of Standards, Washington, U.S. Government Printing Office, 1964.

35. T.M. Apostol, *Mathematical Analysis*, Addison-Wesley, Reading, Mass., 1957.

Appendix A

COMPUTATION OF PARAMETERS FOR SOME OF THE PROBABILITY DENSITIES USED
[Unclassified Title]

VARIANCE OF THE RICE-POWER DISTRIBUTION

(U) We have from Eq. (2.8)

$$E\{\sigma^2\} = \int_0^\infty \sigma^2 \frac{1+m^2}{\bar{\sigma}} \exp(-m^2) \exp\left[-(1+m^2)\frac{\sigma}{\bar{\sigma}}\right] I_0\left(2m\sqrt{(1+m^2)\frac{\sigma}{\bar{\sigma}}}\right) d\sigma$$

$$= e^{-m^2} \frac{\bar{\sigma}^2}{(1+m^2)^2} \int_0^\infty \tau^2 \exp(-\tau) J_0(2im\sqrt{\tau})\, d\tau$$

$$= e^{-m^2} \frac{\bar{\sigma}^2}{(1+m^2)^2} 2\int_0^\infty \lambda^5 e^{-\lambda^2} J_0(2im\lambda)\, d\lambda . \qquad \text{(A1)}$$

Using formula (11.4.28) from p. 486 of Ref. 34, we have

$$\int_0^\infty \lambda^5 e^{-\lambda^2} J_0(2im\lambda)\, d\lambda = \frac{\Gamma(3)}{2\Gamma(1)} M(3, 1, m^2) = M(3, 1, m^2) . \qquad \text{(A2)}$$

From (13.1.27), p. 505, and (13.6.9), p. 509, of Ref. 34,

$$M(3, 1, m^2) = e^{m^2} M(-2, 1, -m^2) = e^{m^2} L_2^{(0)}(-m^2) . \qquad \text{(A3)}$$

From (22.3.9), p. 775, of Ref. 34,

$$L_2^{(0)}(-m^2) = 1 + 2m^2 + \frac{1}{2} m^4 . \qquad \text{(A4)}$$

Using Eqs. (A1–A4), we obtain

$$E\{(\sigma - \bar{\sigma})^2\} = e^{-m^2} \frac{\bar{\sigma}^2}{(1+m^2)^2} (2 + 4m^2 + m^4) e^{m^2} - \bar{\sigma}^2$$

$$= \frac{\bar{\sigma}^2}{(1+m^2)^2} (1 + 2m^2) . \qquad \text{(A5)}$$

MEDIAN OF THE RICE-POWER DISTRIBUTION

(U) The median is by definition the solution of

$$\frac{1}{2} = \int_0^x \frac{1+m^2}{\bar{\sigma}} \exp\left[-m^2 - (1+m^2)\frac{\sigma}{\bar{\sigma}}\right] I_0\left(2m\sqrt{(1+m^2)\frac{\sigma}{\bar{\sigma}}}\right) d\sigma$$

$$= \int_0^{\sqrt{(1+m^2)\frac{x}{\bar{\sigma}}}} 2\tau \exp(-m^2-\tau^2) I_0(2m\tau)\, d\tau . \tag{A6}$$

So to find the median we first solve

$$\frac{1}{2} = \int_0^y 2\tau \exp(-m^2-\tau^2) I_0(2m\tau)\, d\tau \tag{A7}$$

to obtain y, and then the mean to median ratio is given by

$$\rho(m^2) = \frac{\bar{\sigma}}{\sigma_m} = \frac{1+m^2}{y^2} . \tag{A8}$$

First we obtain the mean to median ratio as a function of m^2 using the tabulation in Ref. 26, which permits computation of y. In Ref. 26, the values of y_1 which solve

$$\frac{1}{2} = \int_0^{y_1} 2m^2 r \exp[-m^2(1+r^2)] I_0(2m^2 r)\, dr \tag{A9}$$

are given. If we let $mr = \tau$ in Eq. (A9), we obtain

$$\frac{1}{2} = \int_0^{my_1} 2\tau \exp(-m^2-\tau^2) I_0(2m\tau)\, d\tau . \tag{A10}$$

Comparing Eqs. (A7) and (A10), we see that

$$y = my_1 . \tag{A11}$$

Table A1 gives the necessary computations. The first three columns are from Ref. 26. In Fig. A1, the mean to median ratio as a function of m^2 is plotted.

(U) Table A1—Values of Mean to Median Ratio for the Rice-Power Density as Function of m^2

m^2 (dB)	m^2	y_1	y	$\rho(m^2) = \bar{\sigma}/\sigma_m$
20	100.00	1.0025	10.025	1.005
18	63.096	1.004	7.9751	1.0078
16	39.811	1.0063	6.3493	1.0123
14	25.119	1.0099	5.0615	1.0195
12	15.849	1.0157	4.0436	1.0305
10	10.00	1.0249	3.2410	1.0472
8	6.3096	1.0394	2.6109	1.0723
6	3.9811	1.0622	2.1194	1.1089
4	2.5112	1.0981	1.7401	1.1596
2	1.5849	1.1546	1.4536	1.2234
0	1.000	1.2437	1.2437	1.2930
−2	0.63096	1.3817	1.0975	1.3540
−4	0.39811	1.5860	1.0007	1.3962
−6	0.25119	1.8724	0.93843	1.4208
−8	0.15849	2.2586	0.89917	1.4329
−∞	0.00		0.83255	1.4427

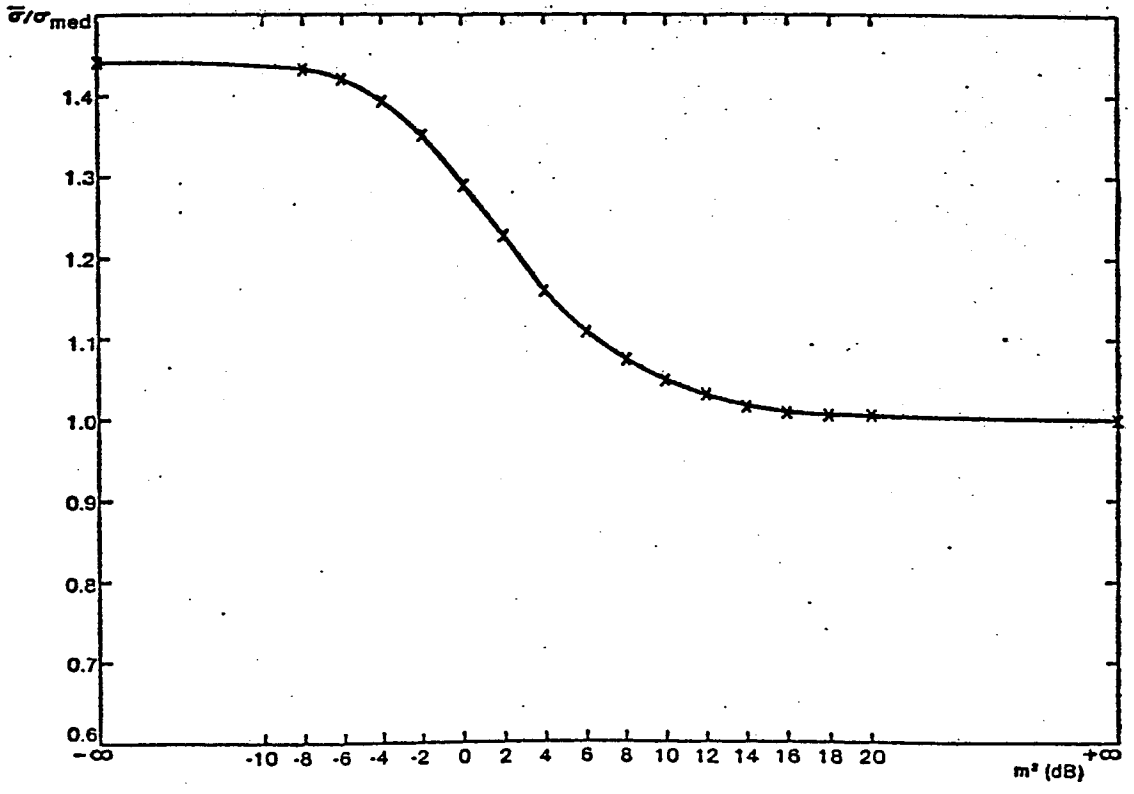

(U) Fig. A1—Mean to median ratio $\rho(m^2)$ as a function of m^2

(U) We now give some analytical results related to the median of this probability density function. Using a series expansion of I_0 in Eq. (A7), we obtain

$$\frac{1}{2} = \int_0^y 2\lambda \exp(-\lambda^2 - m^2) I_0(2m\lambda)\, d\lambda = \sum_{k=0}^{\infty} \int_0^y 2\lambda \exp(-\lambda^2 - m^2) \frac{(m\lambda)^{2k}}{k!k!}\, d\lambda$$

$$= \exp(-m^2) \sum_{k=0}^{\infty} \frac{m^{2k}}{k!} \frac{1}{k!} \int_0^{y^2} \exp(-\tau)\tau^k\, d\tau$$

$$= \exp(-m^2) \sum_{k=0}^{\infty} \frac{m^{2k}}{k!} \left[1 - \exp(-y^2) \sum_{\ell=0}^{k} \frac{y^{2\ell}}{\ell!}\right]$$

$$= 1 - \exp(-m^2) \exp(-y^2) \sum_{k=0}^{\infty} \sum_{\ell=0}^{k} \frac{m^{2k} y^{2\ell}}{k!\ell!}. \tag{A12}$$

Therefore, y, m are related implicitly via the equation

$$\frac{1}{2} \exp(m^2) \exp(y^2) = \sum_{k=0}^{\infty} \sum_{\ell=0}^{k} \frac{y^{2\ell}}{\ell!} \frac{m^{2k}}{k!}. \tag{A13}$$

For $m = 0$, Eq. (A13) gives $\exp(y^2) = 1$, and therefore the pair

$$m = 0, \quad y = \sqrt{\ell n\, 2} = 0.83255 \tag{A14}$$

is an initial value for the functional relationship $y(m)$ we wish to compute. Let

$$F(y, m) = \frac{1}{2} \exp(m^2) \exp(y^2) - f(y, m), \tag{A15}$$

$$f(y, m) = \sum_{k=0}^{\infty} \sum_{\ell=0}^{k} \frac{y^{2\ell}}{\ell!} \frac{m^{2k}}{k!}. \tag{A16}$$

We want to solve

$$F(y, m) = 0 \tag{A17}$$

to obtain y as a function of m. Now

$$\frac{\partial f(y,m)}{\partial y} = \sum_{k=1}^{\infty} \sum_{\ell=1}^{k} \frac{2\ell y^{2\ell-1}}{\ell!} \frac{m^{2k}}{k!} = \sum_{k=1}^{\infty} \sum_{\ell=1}^{k} \frac{2y y^{2(\ell-1)} m^{2k}}{(\ell-1)!k!}$$

$$= 2y \sum_{k=1}^{\infty} \sum_{\ell=0}^{k-1} \frac{y^{2\ell} m^{2k}}{\ell! k!}$$

$$= 2y[f(y,m) - I_0(2my)], \tag{A18}$$

and

$$\frac{\partial f(y,m)}{\partial m} = \sum_{k=1}^{\infty} \sum_{\ell=0}^{k} \frac{y^{2\ell} 2km^{2k-1}}{\ell! k!} = 2m \sum_{k=1}^{\infty} \sum_{\ell=0}^{k} \frac{y^{2\ell} m^{2(k-1)}}{\ell!(k-1)!}$$

$$= 2m \sum_{k=0}^{\infty} \sum_{\ell=0}^{k+1} \frac{y^{2\ell} m^{2k}}{\ell! k!}$$

$$= 2mf(y,m) + 2m \sum_{k=0}^{\infty} \frac{y^{2(k+1)} m^{2k}}{(k+1)!k!}$$

$$= 2mf(y,m) + 2yI_1(2my). \tag{A19}$$

Therefore, since Eq. (A17) holds for the correct functional relationship y, m, we obtain

$$\frac{\partial F(y,m)}{\partial y} = y \exp(m^2) \exp(y^2) - 2yf(y,m) + 2yI_0(2ym)$$

$$= 2yI_0(2ym) \tag{A20}$$

and

$$\frac{\partial F(y,m)}{\partial m} = m \exp(m^2) \exp(y^2) - 2mf(y,m) - 2yI_1(2my)$$

$$= -2yI_1(2my). \tag{A21}$$

From the implicit function theorem [35], there exists a continuously differentiable function $y(m)$ which solves Eq. (A17) and

$$I_0(2my) \frac{dy}{dm} = I_1(2my). \tag{A22}$$

To obtain the functional relationship between y and m, we have to integrate the differential Eq. (A22) with initial condition (A14). Next, observe that

$$f(0, m) = \exp(m^2); \tag{A23}$$

therefore, solving the initial value problem (A18) and (A23), we obtain

$$f(y, m) = \exp(y^2)\exp(m^2) - \int_0^y \exp(y^2 - \sigma^2) 2\sigma I_0(2m\sigma)\, d\sigma . \tag{A24}$$

Since

$$f(y, 0) = 1, \tag{A25}$$

we can solve the initial-value problem (A19) and (A25) to obtain

$$f(y, m) = \exp(m^2) + \int_0^m \exp(m^2 - \sigma^2) 2y I_1(2y\sigma)\, d\sigma$$

$$= I_0(2ym) + \int_0^m 2\sigma \exp(m^2 - \sigma^2) I_0(2y\sigma)\, d\sigma . \tag{A26}$$

Comparing (A24) and (A26), we obtain the identity

$$\exp(y^2)\exp(m^2) - \int_0^y 2\sigma \exp(y^2 - \sigma^2) I_0(2m\sigma)\, d\sigma$$

$$= I_0(2my) + \int_0^m 2\sigma \exp(m^2 - \sigma^2) I_0(2y\sigma)\, d\sigma . \tag{A27}$$

If we now define the probability distribution function

$$P(m, y) = \int_0^y 2\lambda \exp(-\lambda^2 - m^2) I_0(2m\lambda)\, d\lambda , \tag{A28}$$

we can rewrite Eq. (A27) as

$$\exp(y^2)\exp(m^2)[1 - P(m, y)] = I_0(2ym) + \exp(y^2)\exp(m^2) P(y, m) \tag{A29}$$

or

$$P(m, y) + P(y, m) = 1 - \exp(-y^2 - m^2) I_0(2ym) . \tag{A30}$$

We can apply the implicit function theorem again to $P(m, y) = 1/2$ to verify the differential Eq. (A22) obtained earlier.

Appendix B

BACKGROUND AND COMPUTATIONS RELATED TO THE STOCHASTIC PROCESS GENERATION ALGORITHMS
[Unclassified Title]

COMPUTATION OF THE AUTOCORRELATION OF $y_{1,t}^2$

(U) By construction (Eqs. (6.2), (6.3)), the joint probability density of $y_{1,t}, y_{1,t+\tau}$ is

$$P_{y_{1,t}y_{1,t+\tau}}(\psi_1, \psi_2) = \frac{1}{2\pi\left(1 - R_y^2(\tau)\right)} \exp\left(-\frac{1}{2}\,[\psi_1 \psi_2] \begin{bmatrix} R_y(0) & R_y(\tau) \\ R_y(\tau) & R_y(0) \end{bmatrix} \begin{bmatrix} \psi_1 \\ \psi_2 \end{bmatrix}\right), \tag{B1}$$

and the moment-generating function is

$$M(v_1, v_2) = \exp\left(\frac{1}{2}\,[v_1\ v_2] \begin{bmatrix} R_y(0) & R_y(\tau) \\ R_y(\tau) & R_y(0) \end{bmatrix} \begin{bmatrix} v_1 \\ v_2 \end{bmatrix}\right). \tag{B2}$$

Therefore, we compute

$$E\{y_{1,t}^2 y_{1,t+\tau}^2\} = \left.\frac{\partial^4 M(v_1, v_2)}{\partial^2 v_1\, \partial^2 v_2}\right|_{\substack{v_1=0 \\ v_2=0}} = 2R_y^2(\tau) + R_y^2(0). \tag{B3}$$

COMPUTATION OF THE AUTOCORRELATION OF A LOGNORMAL PROCESS

(U) The second-order probability density of y_t is given by Eq. (B1). Then from Eq. (B2) and the definition of the moment-generating function, we have

$$E\{\exp(y_t + y_{t+\tau})\} = E\left\{\exp\left([1\ 1] \begin{bmatrix} y_t \\ y_{t+\tau} \end{bmatrix}\right)\right\}$$

$$= \exp\left(\frac{1}{2}\,[1\ 1] \begin{bmatrix} R_y(0) & R_y(\tau) \\ R_y(\tau) & R_y(0) \end{bmatrix} \begin{bmatrix} 1 \\ 1 \end{bmatrix}\right) = \exp\left[R_y(0) + R_y(\tau)\right]. \tag{B4}$$

COMPUTATION OF THE PROBABILITY DENSITY OF x_t IN EQ. (6.27)

(U) If we let $\Phi_t = \arctan(x_{2,t}/x_{1,t})$, then the joint density of x_t and Φ_t is

$$p_{x_t,\Phi_t}(\xi,\phi) = \frac{1}{\sqrt{2\pi R_g}} \exp\left[-\frac{1}{2R_g}(\xi\cos\phi - c)^2\right]$$

$$\cdot \frac{1}{\sqrt{2\pi R_g}} \exp\left(-\frac{1}{2R_g}\xi^2\sin^2\phi\right)\xi$$

$$= \frac{\xi}{2\pi R_g} \exp\left[-\frac{1}{2R_g}(\xi^2 + c^2 - 2c\xi\cos\phi)\right].$$

Therefore,

$$p_{x_t}(\xi) = \frac{\xi}{2\pi R_g} \exp\left(-\frac{\xi^2 + c^2}{2R_g}\right)\int_{-\pi}^{\pi} \exp\left(\frac{c\xi\cos\phi}{R_g}\right) d\phi$$

$$= \frac{\xi}{R_g} \exp\left(-\frac{\xi^2 + c^2}{2R_g}\right) I_0\left(\frac{c\xi}{R_g}\right), \tag{B5}$$

which is the same as Eq. (2.7) with $\alpha^2 = R_g$.

COMPUTATION OF THE PROBABILITY DENSITY OF x_t^2 IN EQ. (6.28)

(U)

$$p_{\sigma_t}(\sigma) = p_{x_t}(\sqrt{\sigma})\,\frac{1}{2\sqrt{\sigma}} = \frac{1}{2R_g} \exp\left(-\frac{\sigma + c^2}{2R_g}\right) I_0\left(\frac{c\sqrt{\sigma}}{2R_g}\right). \tag{B6}$$

Let

$$m^2 = \frac{c^2}{2R_g} = \frac{\text{steady power}}{\text{average random power}}; \tag{B7}$$

we compute

$$\bar{\sigma} = \int_0^{\infty} \sigma p_{\sigma_t}(\sigma)\, d\sigma,$$

$$= \exp\left(-\frac{c^2}{2R_g}\right)\int_0^{\infty} \frac{\sigma}{2R_g} \exp\left(-\frac{\sigma}{2R_g}\right) I_0\left(\frac{c\sqrt{2}}{\sqrt{R_g}}\,\frac{\sqrt{\sigma}}{\sqrt{2R_g}}\right) d\sigma,$$

$$= 4R_g \exp\left(-\frac{c^2}{2R_g}\right)\int_0^{\infty} \tau^3 \exp(-\tau^2) I_0\left(\frac{c\sqrt{2}}{\sqrt{R_g}}\,\tau\right) d\tau,$$

(using (11.4.28) from Ref. 34, p. 486)

$$= 2R_g \exp\left(-\frac{c^2}{2R_g}\right) M\left(2, 1, \frac{c^2}{2R_g}\right),$$

(using (13.1.27) from Ref. 34, p. 505, and (13.6.9) from Ref. 34, p. 509)

$$= 2R_g \exp\left(-\frac{c^2}{2R_g}\right) \exp\left(\frac{c^2}{2R_g}\right)\left(1 + \frac{c^2}{2R_g}\right)$$

$$= 2R_g(1 + m^2)\,. \qquad \text{(B8)}$$

In view of Eq. (B8), we rewrite Eq. (B6) as

$$p_{\sigma_t}(\sigma) = \frac{1 + m^2}{\bar{\sigma}} \exp\left[-m^2 - (1 + m^2)\frac{\sigma}{\bar{\sigma}}\right] I_0\left(2m\sqrt{(1 + m^2)\frac{\sigma}{\bar{\sigma}}}\right), \qquad \text{(B9)}$$

which is the same as Eq. (2.8).